Phase relations between orbital forcing and climate response in the equatorial Atlantic between 9 and 10 Ma.

Master thesis by

J.A.J. de Jonge

Faculty of Geosciences
Earth Sciences Institute
Master Program: Biogeology
Supervisors: F.J. Hilgen and C. Zeeden

Universiteit Utrecht

Cover photo: Monte dei Corvi section, Italy.

Contents

Phase relations between orbital forcing and climate response in the equatorial Atlantic between 9 and 10 Ma.

J.A.J. de Jonge
Utrecht University, the Netherlands

Abstract

The reconstruction of phase relations between orbital forcing and climate response in the Miocene is hampered by uncertainties in the values for the tidal dissipation and the dynamical ellipticity, which affect lags and leads calculated from paleoclimatic records. Here we aim to solve this problem by generating high resolution physical property data (magnetic susceptibility and color) and isotope data ($\delta^{18}O$ and $\delta^{13}C$) of benthic foraminifera from Ceara Rise in the equatorial Atlantic (ODP Leg 154, Site 926) and using the sapropel bearing Monte dei Corvi section in Italy, for which a direct response can be assumed, to select the proper solution. The precession and obliquity phases of the Ceara Rise data relative to different orbital solutions are determined, and compared with existing younger datasets. Additionally, the effect of changing the tidal dissipation parameter on the phase relations for this time interval is explored. The main conclusions are that the tuning to the $La2004_{(1,1.135)}$ p-.5t maxima or to the $La2004_{(1,1.16)}$ p-.5t maxima gives the most reasonable phase relations for Ceara Rise and that slightly changing the tidal dissipation parameter does not have much effect on the determination of phase relations between 9 to 10 Ma. Also concluded is that the Ceara Rise data lag the Monte dei Corvi data by 57 ± 16 degree at the obliquity band. This lag is probably caused by deep water currents from the southern ocean containing a delayed obliquity signal. Furthermore, it seems that over time the phase between magnetic susceptibility and benthic $\delta^{18}O$ remained relatively constant. However, the phase of the magnetic susceptibility as tuning target might have changed.

1. Introduction

This study is about orbital tuning and phase relations in the Middle Miocene (9-10 Ma). Phase relations between changes in insolation and deep sea temperature response (as a proxy for global climate and ice volume) are constrained for the Pliocene/Pleistocene, but further back in time the lack of accuracy of the geologic timescale did not allow for the determination of time lags. The reconstruction of phase relations between orbital forcing and climate response in the Miocene is held back by uncertainties in the values for the tidal dissipation (td) and the dynamical ellipticity (de), which affect lags and leads calculated from paleoclimatic records. As high resolution orbital solutions become available for the Miocene (Laskar et al., 1993; Laskar et al., 2004), the aim of this study is to overcome this problem and select the proper solution for the interval between 9 and 10 Ma.

High resolution physical property data (color, magnetic susceptibility, which are tuned to changes in insolation) and isotope data ($\delta^{18}O$ and $\delta^{13}C$, as a proxy for deep sea temperature and ice volume) of benthic foraminifera from Ceara Rise in the equatorial Atlantic (ODP Leg 154, Site 926) are generated and the sapropel bearing Monte dei Corvi section in Italy, for which a direct response can be assumed, is used to select the proper solution. The effect of changing the tidal dissipation parameter is investigated and phase relations between the proxies are determined for the first time in the Miocene.

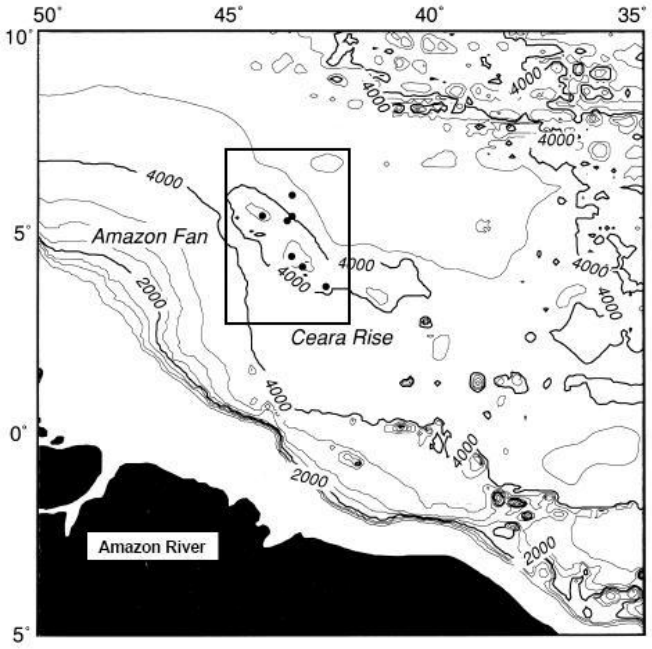

Figure 1. Map showing location and depth of Ceara Rise ODP Site 926, indicated in red, modified from Harris et al. (1997).

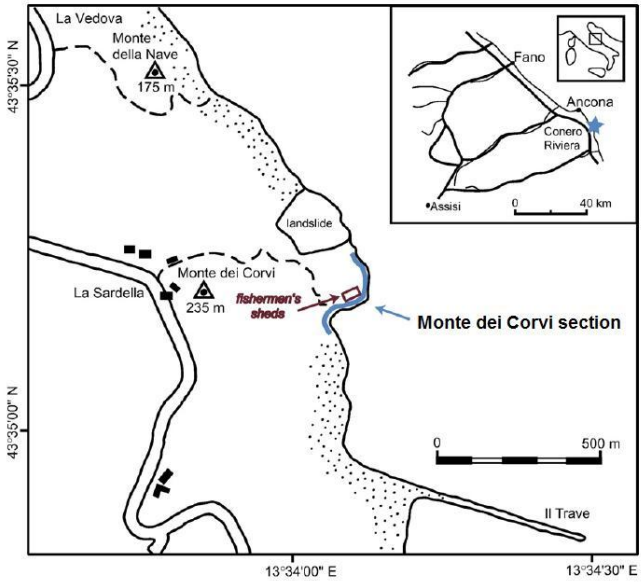

Figure 2. Map showing location of the Monte dei Corvi section, indicated in blue, modified from Hüsing et al. (2007).

The physical property data from the Ceara Rise and the Mediterranean (Monte dei Corvi section) are compared to get constraints of the accuracy of the available timescale. The main findings of the phase relations with obliquity are compared with existing younger datasets (Shackleton and Hall, 1997; Shackleton and Crowhurst, 1997; Tiedemann and Franz, 1997).

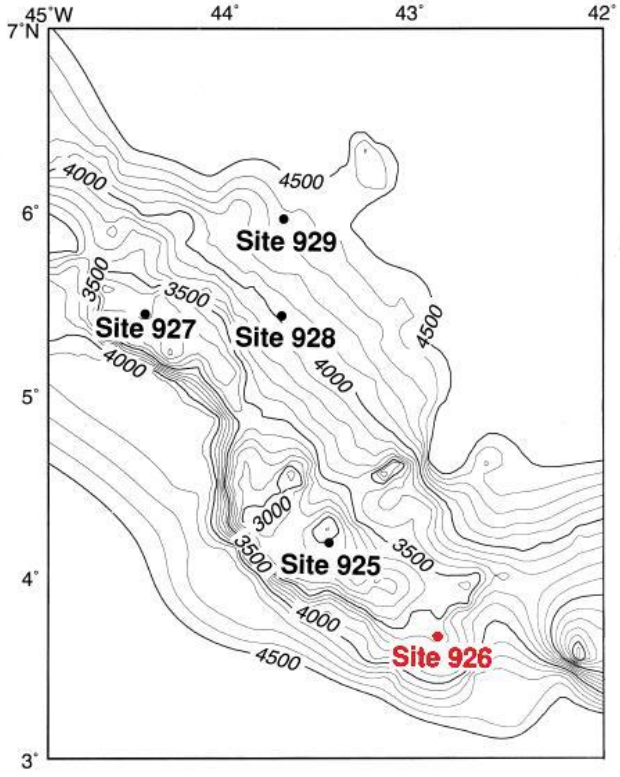

hole	latitude	longitude	water depth (m)
926A	3°43.146′ N	42°54.489′ W	3598.4
926B	3°43.148′ N	42°54.507′ W	3598.3
926C	3°43.130′ N	42°54.508′ W	3598.3

Table 1. Location of the ODP Leg 154 Site 926, modified from Shackleton et al. (1999).

2. Geological settings and sections

In this study two sites are investigated: Ceara Rise OPD Site 926 and the Monte dei Corvi section (Fig. 1 and 2). The Monte dei Corvi section is exposed along the Adriatic coast, 5 km SE of Ancona (43.35.12N; 13.34.10E, Italy). It is a pelagic and hemipelagic carbonate succession and is characterized by cyclic alternations of brown sapropels, white-grayish limestones and greenish-grey marls (Hüsing et al., 2007). Ceara Rise ODP Site 926 is located in the western equatorial Atlantic and was drilled during Ocean Drilling Program (ODP) Leg 154 (Table 1). It includes well-preserved cores through most of the Miocene. The sediments mostly consist of whitish biogenic carbonate,

mainly produced by calcareous plankton, and reddish terrigenous clays and quartz, transported from the Amazon and other rivers (Harris et al., 1997). Trace amounts of terrigenous material may further come from Africa by eolian transport (Balsam et al., 1995).

3. Material and methods

3.1 Monte dei Corvi

3.1.1 Color measurements

During a fieldwork, in May 2011, high resolution (ca. 2cm spacing) color measurements have been performed on the Miocene part of the Monte dei Corvi section, Italy. This resolution was chosen, because at least 10 samples per precession related cycle were needed to obtain a useful quantitative record of the astronomically forced cyclicity. Using a Jacob staff and compass, stratigraphic thicknesses were measured every 40 cm and the sample spacing was calculated and marked. Using the Konica Minolta portable CM-600d spectrometer the color of the sediment was measured at the wet rock surface. Where necessary due to weathering, fresh rock was exposed by hammering. The data represent averages of 3 measurements each per sample level.

3.2 Ceara Rise

3.2.1 Sampling

This study is partly based on sediments recovered during Ocean drilling Program (ODP) Leg 154 on the Ceara Rise, including the well-preserved section through the upper Miocene at Site 926. Detailed correlations between the A, B and C holes are made by C. Zeeden (in prep.), using magnetic susceptibility data and high resolution core photographs which show cyclic patterns in the sediment. At the MARUM, Center for marine environmental sciences, University of Bremen, samples were taken from the three Holes at approximately 4 cm spacing for the interval between 9 and 10 Ma. Slumps were taken into account and an overlap was sampled at the transition from the A to the B Hole. 191 samples were taken from Hole 926A, 91 from Hole 926B and 104 from Hole 926C. Approximately 15 meter core was sampled. Sample positions, physical properties and isotope data are listed in appendix 2.

3.2.2 Physical properties

At the Utrecht University color measurements were performed on all the Ceara Rise samples, using a Konica Minolta portable CM-600d spectrophotometer. The spectrophotometer measured color at 29 different frequencies. After the color measurements, the samples were weighted and freeze-dried.

The magnetic susceptibility of the Ceara Rise samples was measured using a Kappabridge KLY-2 at the paleomagnetic lab in Fort Hoofddijk, Utrecht. After weighing all the samples the susceptibility values were divided by their weight, resulting in the specific susceptibility.

3.2.3 Isotope analysis and sample preparation

To avoid contamination, before washing and sieving the samples, the residue of the liquid used during core drilling was scraped off the outside of the samples. After this the sediments were placed in a beaker containing distilled water which helps the sediments to disintegrate. Only distilled water was used in the beakers, because tap water contains calcium carbonate that can precipitate on the foraminifers which can result in an error in the stable isotope data.

First using tap water, followed by thoroughly rising with distilled water, the sediments were sieved into four fractions: >355 µm, 250-355 µm, 150-250 µm and 63-150 µm. The sieves were each time cleaned before starting a new sample. After sieving, the residues were oven dried at 40 °C and contained almost only foraminifers. When dry, the foraminifers were stored, using a small brush and pieces of paper, in glass files.

If possible the 250-355 µm fraction was used for picking the foraminifers. If there were not enough foraminifers in this fraction, picking continued in the lager fraction (>355 µm) and if still not enough foraminifers, then picking continued in the 150-250 µm fraction. Two species of foraminifers were picked: *Cibicidoides mundulus* and *Planulina wuellestorfi* (Holbourn et al., 2007). After picking, based on how well they were preserved, the best foraminifers were selected. The amount of selected foraminifers varied between 1 to 7. After selecting, the foraminifers were put in a small plastic jar with a pit in the middle. The samples containing more than 1 foraminifer were crushed under the microscope using a metal paperclip. The samples containing only a single foraminifer were not crushed because the weight could become too low for stable isotope measurements. Then the samples were cleaned by adding ethanol in the jar and holding it in an ultrasonic bath for approximately 1.5 second. When the foraminifer parts were clean enough, the ethanol was poured in a beaker leaving the foraminifer parts in the small jar. Overnight the small jars were oven dried at 35 °C.

The stable isotope measurements were made on a CARBO-KIEL automated carbonate preparation device linked online to a Finnigan MAT253 mass spectrometer at Utrecht University. The results were calibrated using the international standard NBS-19 and in-house standard Naxos. The analytical precision was better than 0.04‰ and 0.08‰ for d13C and d18O, respectively. Values are reported in standard delta notation (d) relative to Vienna Pee Dee Belemnite (VPDB) (trough personal communication with A. van Dijk).

3.3 Spectral analysis

To detect cyclic patterns and create phase plots, Cross Blackman-Tukey spectral analysis of the AnalySeries program 1.1.1. was applied on the color data of the Monte dei Corvi in the time domain. For the Ceara Rise, these analyses were applied on the magnetic susceptibility, $\delta^{18}O$, $\delta^{13}C$ and on the color data in the depth and in the time domain. For the coherency a confidence level of 95% is used.

4. Data description

4.1 Monte dei Corvi

Figure 3 shows the raw Monte dei Corvi color data in depth. The color is measured as lightness (L*D65) so higher values mean light colored sediments and low values mean dark colored sediments. The color record shows regular, distinct and narrowly spaced peaks reaching minimum values of ± 35 in the lower 2.5-3 meter of the section. From 3 meter upwards, the peaks abruptly become more prominent and widely spaced, and reach values between 35 and 25. These peaks often alternate with much weaker peaks. The wider spacing continues up to 14 meter, but is interrupted twice by peaks that reveal again a narrower spacing (at 6 and 10 meter). The upper 4 meter is again marked by distinct peaks which show a regular and more narrow spacing, although the distance between the peaks is larger than in the lower part of the section.

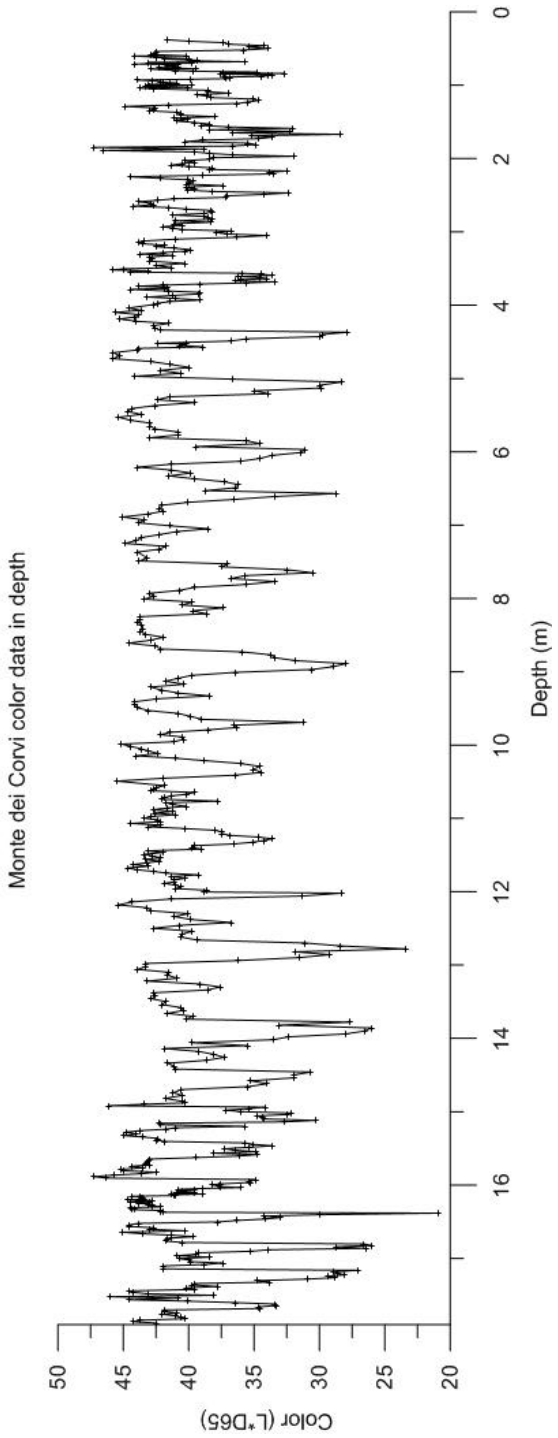

Figure 3. Monte dei Corvi color data, presented as raw data vs. composite depth. Dots indicate sample positions.

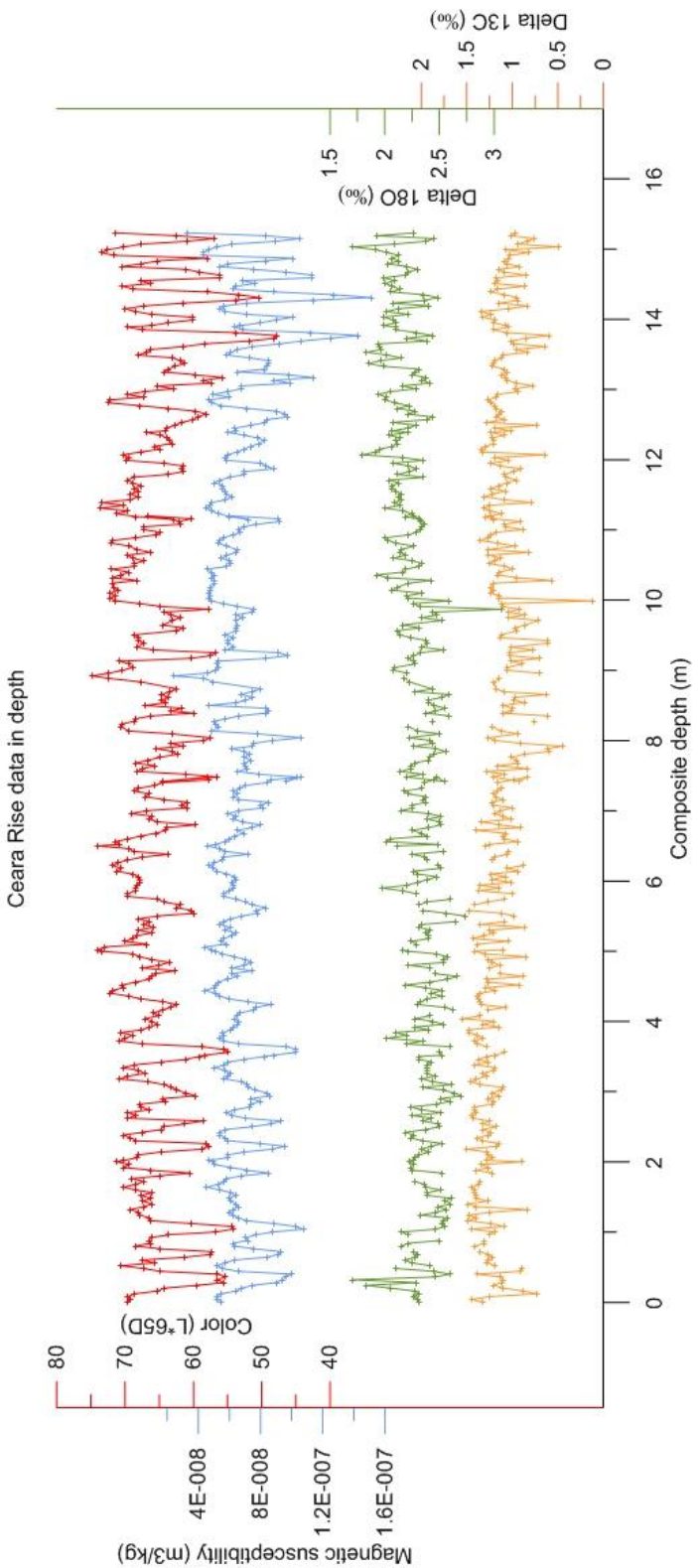

Figure 4. Ceara Rise magnetic susceptibility (blue), color (red), benthic oxygen (green) and carbon isotope (orange) data, presented as raw data vs. composite depth. Dots indicate sample positions.

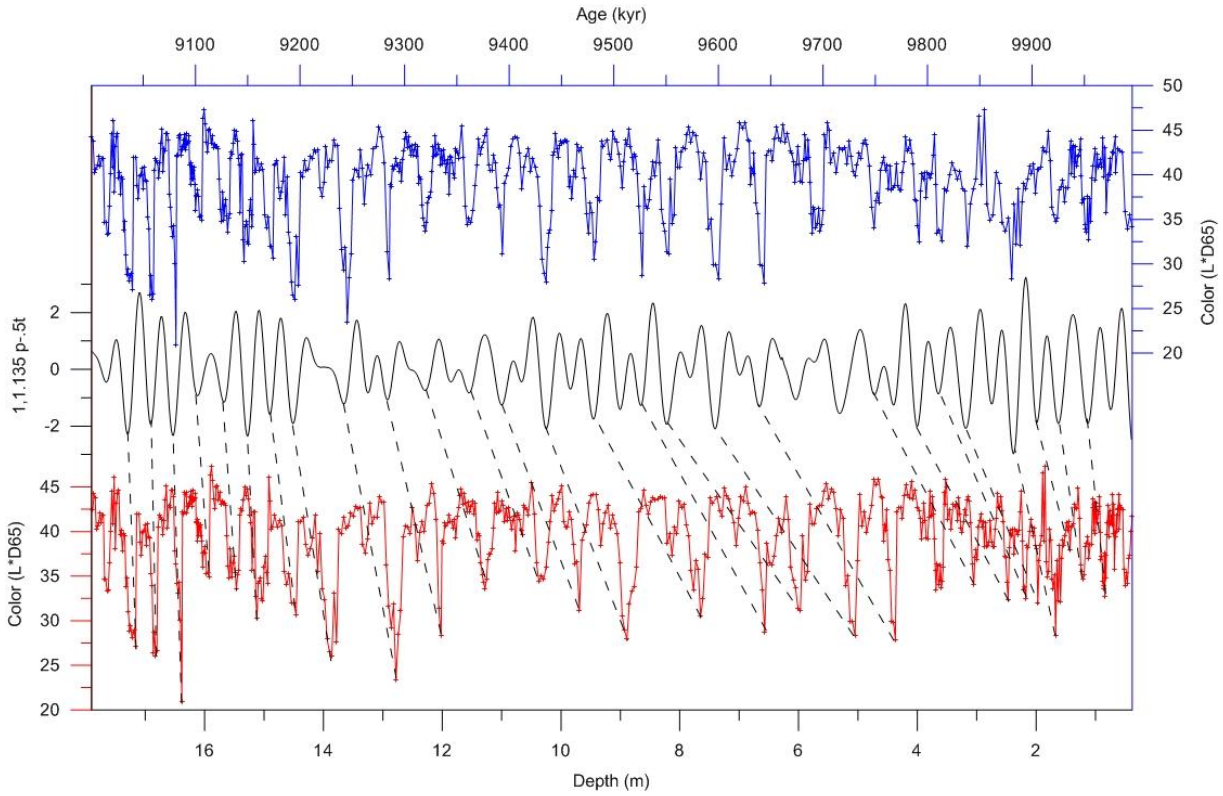

Figure 5. Tuning of Monte dei Corvi color record to La2004*(1,1.135)* p.-5t. Red indicates color data in the depth, blue indicates color data in the time domain. Dashed lines indicate tie points. Not all tie points are indicated.

4.2 Ceara Rise

Figure 4 shows the raw magnetic susceptibility, color, $\delta^{18}O$ and $\delta^{13}C$ data of the Ceara Rise against depth. It can be seen that the magnetic susceptibility and the color data show almost exactly the same pattern but are in anti-phase (axis values for magnetic susceptibility are in reversed order). The $\delta^{18}O$ data of the benthic foraminifers also shows a clear cyclic pattern, which seems in-phase with magnetic susceptibility but shifted a bit, so that $\delta^{18}O$ maxima appear to lead magnetic susceptibility maxima. The $\delta^{13}C$ data only shows a cyclic pattern between 7.5 and 14 meter however, this pattern cannot easily be correlated to the data of the other three proxies.

5. Astronomical age model

To find a reliable solution for precession and obliquity Laskar et al. (1993) incorporated two variables namely dynamical ellipticity of the earth and tidal dissipation by the moon. Present day values of these parameters are set at 1 and changing them yields different precession/obliquity interference patterns (Hüsing et al., 2007). To maintain an excellent fit with older cyclostratigrophic records it is clear that the parameters have to be modified (Pälike and Shackleton, 2000). In this study, the data of the Monte dei Corvi and the data of the Ceara Rise will be compared to orbital time series of La2004, using different tidal dissipation values.

5.1 Monte dei Corvi

Hüsing et al. (2007) tuned the cyclic alternations of brown sapropels, white-grayish limestones and greenish-grey marls of the Monte dei Corvi section to the La2004*(1,1)* solution for the time interval between 5 and 14 Ma. They already realized that the

		Phase relation obliquity (°)
Age model	Orbital solution	MS*
1	Laskar2004$_{(1,1)}$ p-.5t minima	157 ± 4
2	Laskar2004$_{(1,1)}$ p-.5t maxima	43 ± 14
3	Laskar2004$_{(1,1.135)}$ p-.5t minima	138 ± 5
4	Laskar2004$_{(1,1.135)}$ p-.5t maxima	22 ± 11
5	Laskar2004($_{(1,1.16)}$ p-.5t maxima	23 ± 9
*Positive values lag solution.		

Table 2, Different Ceara Rise age models and phase relation at the obliquity band.

La2004$_{(1,1)}$ record did not fit the geological record of the Monte dei Corvi well, and partly suggested a tuning to the La2004$_{(1,1.2)}$ or La2004$_{(1,0.5)}$ solution. In this study their original log, for the interval between 9 and 10 Ma, was slightly modified based on our observations in the field. The sapropel layers of Monte dei Corvi are directly linked to maximum African monsoon intensities as a consequence of stronger boreal summer insolation that result from precession minima and obliquity maxima (Ziegler et al., 2010). Transient climate modeling results indicate an in-phase behavior/direct response of the African monsoon relative to astronomical forcing (Tuenter et al., 2005). So for the Monte dei Corvi the filtered precession related signal of the high resolution color record was tuned to precession and cross-spectral analysis was applied to calculate the lead/lag with respect to obliquity. An in-phase relation with obliquity was translated to a tidal dissipation value (Zeeden et al., in prep.). The interval of 9 to 10 Ma is located in a 2.4 Myr eccentricity minimum which resulted in the most prominent interference patterns and the results showed that the La2004$_{(1,1.135)}$ p-.5t is the right solution for tuning the Monte dei Corvi color record (Fig. 5).

5.2 Ceara Rise (Table 2)

For the tuning of Ceara Rise, the magnetic susceptibility maxima of the samples were used, because the maxima better reflect the amplitude of the astronomical forcing and are less affected by background noise than the minima (Shackleton and Crowhurst, 1997). Five different age models were established. Present day values for the dynamical ellipticity and tidal dissipation are used for tuning the first two age models (La2004$_{(1,1)}$ p-.5t). These present day values are used to determine if the tuning of the Ceara Rise record to the La2004$_{(1,1)}$ does not give the best results and to see the difference in results when changing the tidal dissipation value. For the first age model the magnetic susceptibility maxima were tuned to the La2004($_{(1,1)}$ p-.5t minima and for the second age model the magnetic susceptibility maxima were tuned to the La2004($_{(1,1)}$ p-.5t maxima.

The third and fourth age models are based on the tuning to La2004$_{(1,1.135)}$ p-.5t. This solution is selected because at Monte dei Corvi the tuning of the easily recognizable sapropel layers, which show a direct response to astronomical forcing, indicated that the La2004$_{(1,1.135)}$ p-.5t is the right solution for the interval between 9 and 10 Ma. The magnetic

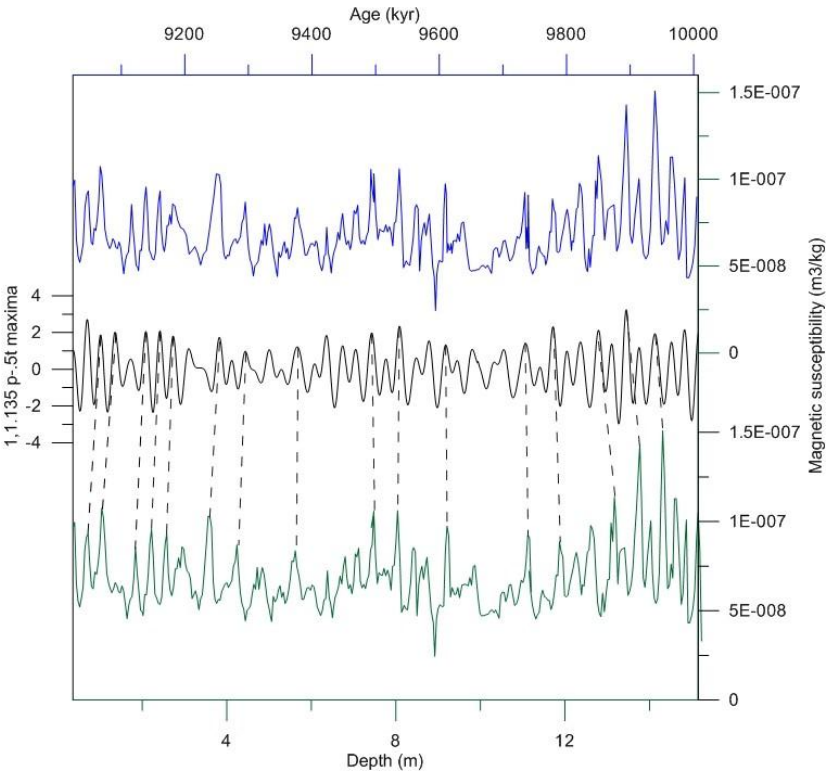

Figure 6. Tuning of the Ceara Rise magnetic susceptibility record to La2004$_{(1,1.135)}$ p.-5t maxima. Green indicates color data in the depth, blue indicates color data in the time domain. Dashed lines indicate tie points, not all used tie points are indicated.

susceptibility maxima in the third age model, were correlated to La2004$_{(1,1.135)}$ p-.5t minima and in the fourth age model to La2004$_{(1,1.135)}$ p-.5t maxima (Fig. 6).

During the process of making the phase plots a new method for tuning data to the right solution was developed by C. Zeeden (in prep.). When looking at the tuning of the data to the La2004$_{(1,1)}$ solution, lags and leads of the obliquity cycle could be calculated. These lags/leads could be used to calculate a tidal dissipation value and resulted in a fifth age model. In this fifth age model the magnetic susceptibility maxima are tuned to La2004$_{(1,1.16)}$ p-.5t maxima. The magnetic susceptibility, color, $\delta^{18}O$ and $\delta^{13}C$ data of Ceara Rise are presented as raw data versus time, using the La2004$_{(1,1.16)}$ p-.5t, in Figure 7.

6. Phase relations

6.1 Ceara Rise

After generating the age models for Ceara Rise, phase plots were created. Figure 8 shows the phase plots for Ceara Rise containing only the data from hole A. Here only the A hole was used because it has the most constant sedimentation rate. In the first tree plots (Fig 8a-c) the results of the cross-spectral analyses between magnetic susceptibility and color, and benthic oxygen and carbon isotope data are shown in the depth domain. Looking at Figure 8a, it can be seen that magnetic susceptibility and color are in anti-phase. So when the magnetic susceptibility is high, the average L*(D65) is low. This is correct because higher magnetic susceptibility values coincide with darker sediments, and darker sediments have lower average lightness values (Average L*(D65)).

Looking at the $\delta^{18}O$ data in the depth domain it can be assumed that a period of approximately 0.35 meter corresponds to the precession cycle and a period around 0.6 meters to obliquity (Fig. 8b). No significant power is found at the eccentricity band of the spectrum, because the interval of 9 to 10 Ma is located in a 2.4 Myr eccentricity minimum. In the depth domain, the phase relation between magnetic susceptibility and benthic $\delta^{18}O$ is approximately in-phase for obliquity (a ± 7 degree phase lag at the highest coherency), while magnetic susceptibility

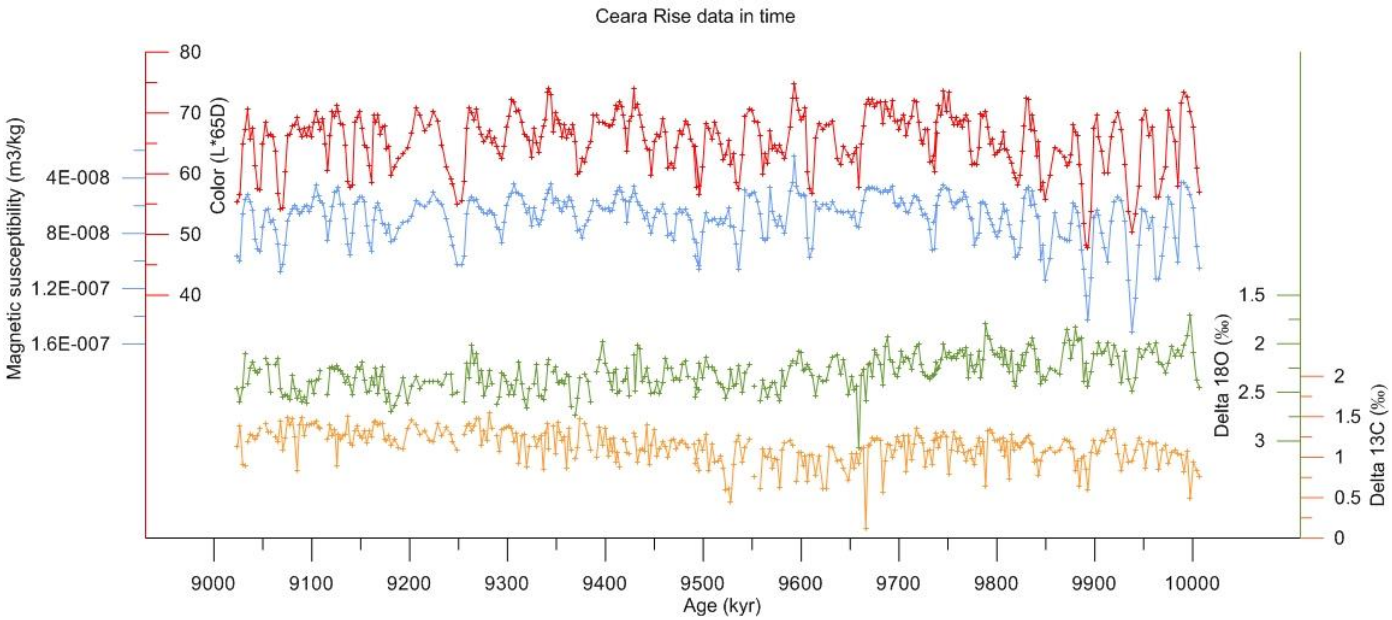

Figure 7. Ceara Rise magnetic susceptibility (blue), color (red), benthic $\delta^{18}O$ (green) and $\delta^{13}C$ (orange) data, presented as raw data vs. time using La2004$_{(1,1.16)}$ p-.5t maxima. Dots indicate sample positions.

leads $\delta^{18}O$ with 33 degree in the precession band. For obliquity, it implies that high magnetic susceptibility values coincide with high $\delta^{18}O$ values.

Figure 8c shows the phase relations between magnetic susceptibility and the benthic $\delta^{13}C$ in the depth domain. At a period of 0.6 meter, $\delta^{13}C$ is almost out of phase (± -163 degrees) with magnetic susceptibility. At a period of 0.41 meter, the phase is ± -53 degrees, but the coherency is very low.

To compare the results in the depth domain with the results in the time domain, Figure 8 also shows the phase plots using the tuning to La2004$_{(1,1)}$ p-.5t maxima, La2004$_{(1,1.135)}$ p-.5t maxima and the La2004$_{(1,1.16)}$ p-.5t maxima, and only the A Hole data. Figures 8d-f show the phase plots of magnetic susceptibility vs. stable isotopes and color tuned to the La2004$_{(1,1)}$ p-5t maxima. Figure 8g-i show the phase plots of magnetic susceptibility vs. stable isotopes and color tuned to the La2004$_{(1,1.135)}$ p-5t maxima and Figures 8j-l show the phase plots of magnetic susceptibility vs. the stable isotopes and color tuned to the La2004$_{(1,1.135)}$ p-5t maxima. The color shows the same anti-phase relation with magnetic susceptibility in the time domain as in the depth domain with high coherencies for all periods. Looking at the $\delta^{18}O$ plots it can be observed that the 0.35 meter cycle in the depth domain indeed corresponds to the 23 kyr precession cycle in the time domain. The same is true for the 0.6 meter cycle which corresponds to the 41 kyr obliquity cycle. Looking at the $\delta^{13}C$ plots, the results in the time domain are very different from the results in the depth domain. The coherencies in the time domain are very low. Despite the fact that the obliquity cycle is clearly visible in the raw carbon data, somewhat higher coherencies could only be found at a period of approximately 63 kyr. Looking closer at the $\delta^{13}C$ phase plots (Fig 8f,i,l), it is observed that only very weak peaks are present at approximately 38 and 18 kyr, when using the 1,1 solution. No obliquity peak is found when the 1,1.135 and 1,1.16 solutions are used and only a small peak is found at 18 kyr in case the 1,1.135 solution is used. A possible reason for this is that a significance level of 95% is used. Probably precession and obliquity peaks would have reached higher coherencies if a lower significance level and not only the data of the A Hole but all the data had been used.

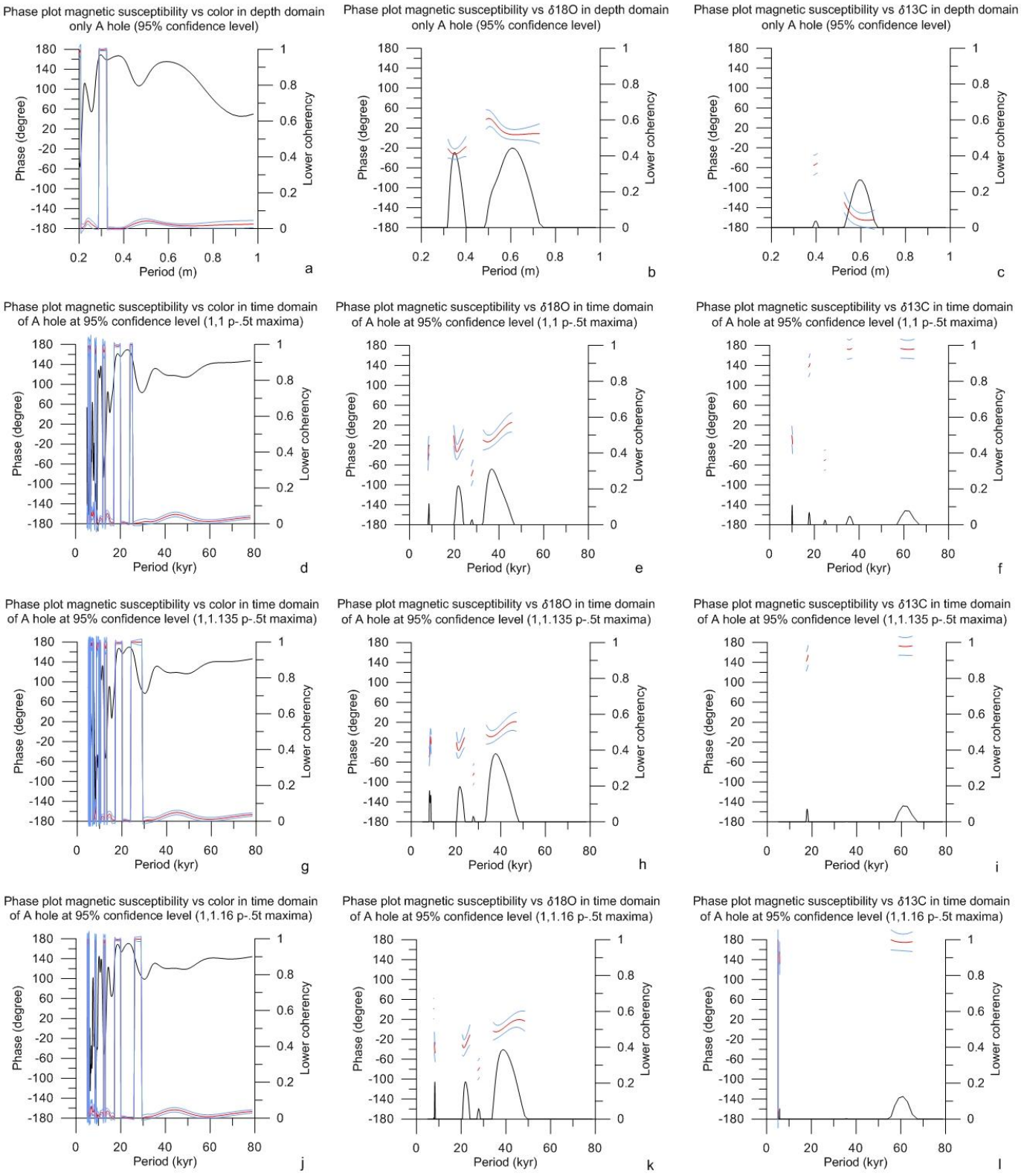

Figure 8. Phase plots of the Ceara Rise data containing only the data from the A hole. A-c, data is plotted in depth domain. D-f, data is plotted vs. La2004$_{(1,1)}$p-.5t maxima. G-i, data is plotted vs. La2004$_{(1,1.135)}$p-.5t maxima. J-l, data is plotted vs. La2004$_{(1,1.16)}$ p-.5t maxima. Black line indicates lower coherency, red line indicates phase, blue lines indicate upper and lower phase. Negative values indicated phase lead and positive values indicate a phase lag with the orbital solution.

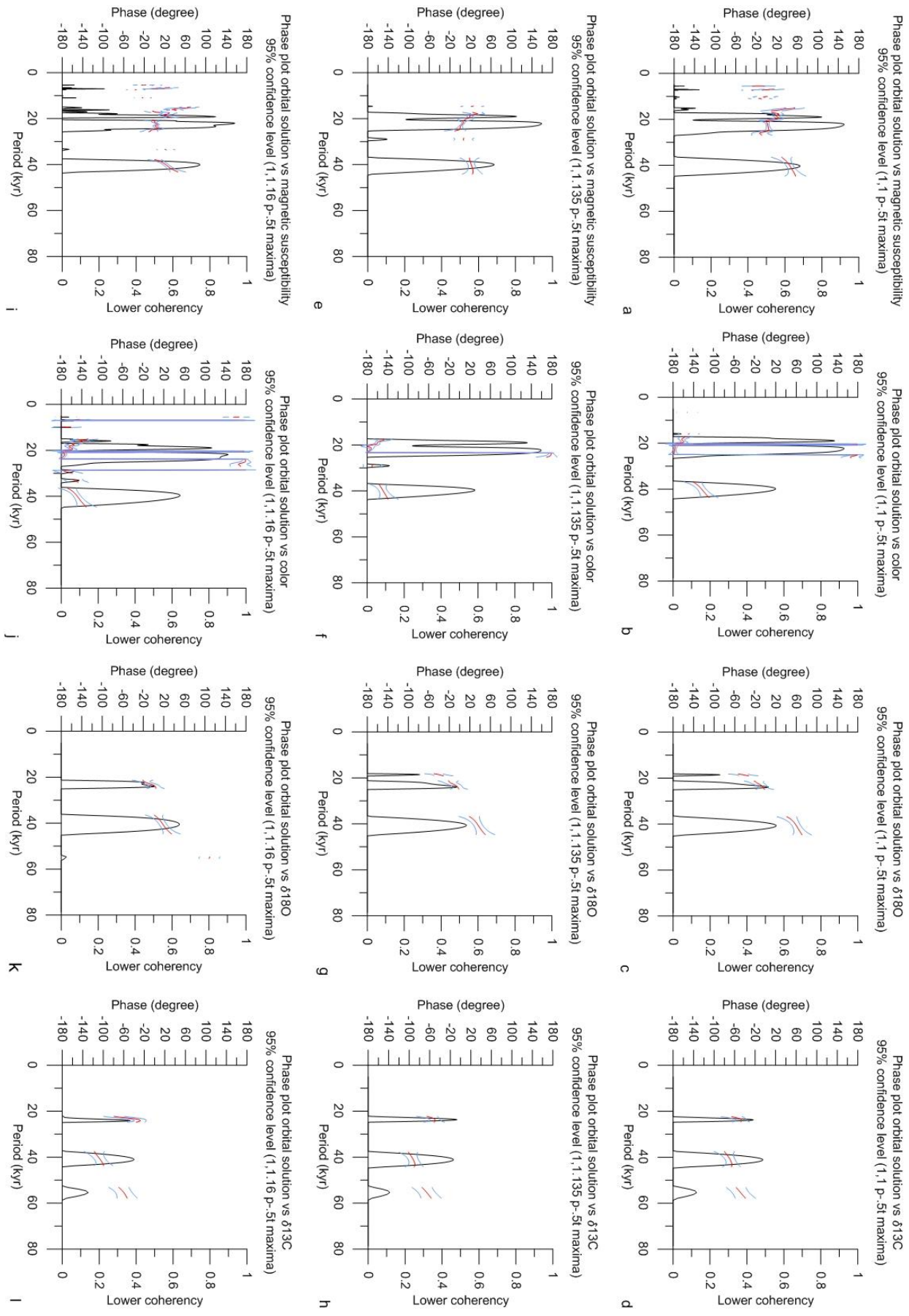

Figure 9. Phase plots of the Ceara Rise data containing all data. A-d, data is plotted vs. La2004$_{(1,1)}$ p-.5t maxima. E-h, data is plotted vs. La2004$_{(1,1.135)}$ p-.5t maxima). i-l, data is plotted vs. La2004$_{(1,1.16)}$p-.5t maxima. Black line indicates lower coherency, red line indicates phase, blue lines indicate upper and lower phase. Negative values indicated phase lead and positive values indicate a phase lag with the orbital solution.

		Magnetic susceptibility			Color			Oxygen			Carbon		
La2004	Cycle (kyr)	19	23	40	19	23	40	19	23	40	19	23	40
1,1.135 p-.5t	phase (degree)	-154 ± 24	-172 ± 3	138± 10	29 ± 15	6 ± 11	-32 ± 10	143± 20	171 ± 14	137 ± 10	-	113± 15	-22 ± 13
P Min. O Max.	phase (kyr)	-8 ± 1.5	-11± 0.5	15.5 ± 1	1.5 ± 1	0.5 ± 0.5	-3.5± 1	7.5 ± 1	11 ± 1	15 ± 1	-	7 ± 1	-2.5 ± 1.5
1,1.135 p-.5t	phase (degree)	20 ± 12	3 ± 7	22 ± 11	-160 ± 11	-176 ± 6	-150 ± 14	-40 ± 15	-5 ± 18	36 ± 14	-	-50 ± 17	-92 ± 14
P Max. O Min.	phase (kyr)	1 ± 0.5	0 ± 0.5	2.5 ± 1	-8.5 ± 0.5	-11 ± 0.5	-16.5± 1.5	-2 ± 1	-0.5 ± 1	4 ± 1.5	-	-3 ± 1	-10.5± 1.5
1,1.16 p-.5t	phase (degree)	25 ± 10	3 ± 8	23 ± 9	-161 ± 10	-173 ± 7	-150 ± 12	-	-5 ± 14	18 ± 11	-	-28 ± 33	-107 ± 15
P Max. O Min.	phase (kyr)	1.5± 0.5	0 ± 0.5	2.5 ± 1	-8.5 ± 0.5	-10.5± 0.5	-16.5± 1.5	-	-0.5 ± 1	2 ± 1	-	-2 ± 2	-12 ± 1.5

Table 3. Phase lags/leads of the Ceara Rise data, calculated using only the highest coherencies of the La2004$_{(1,1.135)}$ p.-5t minima, the La2004$_{(1,1.135)}$ p.-5t maxima and the La2004$_{(1,1.16)}$ p.-5t maxima. Negative values indicated phase lead and positive values indicate a phase lag with the orbital solution.

In Figure 8 it can further be seen that the results based on the tuning to the La2004$_{(1,1.135)}$ p-.5t and La2004$_{(1,1.16)}$ p-.5t maxima are almost identical. To get a better insight in the phase lags/leads and to determine which age model gives the most reasonable results, Figure 9 shows the phase plots between all the magnetic susceptibility, color and stable isotope data, so using the data from all 3 Holes, and the different astronomical solutions. Here the phase plots for the tuning to the 1,1 solution are only shown for comparison. Looking at plots for both the La2004$_{(1,1.135)}$ p-.5t and the La2004$_{(1,1.16)}$ p-.5t maxima, it can be seen that for magnetic susceptibility high coherencies are reached at 19 and 23 kyr, corresponding to the main precession components, and at 41 kyr, corresponding to the obliquity cycle. There are also peaks at different periods, these are not taken into account because the coherencies are very low. Appendix 1i-l also shows these phase plots based on the tuning to La2004$_{(1,1.135)}$ p-.5t minima. Again high coherencies are found in the precession and obliquity band. Table 3 lists the phase lags and leads for these three orbital solutions.

6.2 Monte dei Corvi and comparison

Figure 10 shows the phase plots of the Monte dei Corvi color data vs. three different solutions (La2004$_{(1,1)}$, La2004$_{(1,1.135)}$ and La2004$_{(1,1.16)}$ p-.5t maxima). No plots are made for the tuning to La2004$_{(1,1.135)}$ p-.5t minima, but this will probably not give very different results, although the phase relation with respect to precession and obliquity will be opposite. Again the 1,1 solution is only plotted for comparison but is not included in the phase relation Table. In the Monte dei Corvi data also the two precession cycles and the 40 kyr obliquity cycle are clearly visible in the outcome of the cross-spectral analysis. At the Monte dei Corvi the dark brown to black Sapropels are related to precession minima and obliquity maxima. So for the tuning of the Monte dei Corvi the L*D65 *minima* are correlated to La2004$_{(1,1.135)}$ p-.5t and La2004$_{(1,1.16)}$ p-.5t *minima*.

		Color data Monte dei Corvi			Color data Ceara Rise			Cross-spectral comparison Monte dei Corvi and Ceara Rise		
La2004	Cycle (kyr)	19	23	40	19	23	40	19	23	40
1,1.135 p-.5t	phase (degree)	11 ± 14	-2 ± 16	-24 ± 10	20 ± 11	4 ± 6	30 ± 14	16 ± 16	6 ± 11	57 ± 16
P min. O max.	phase (kyr)	0.5 ± 0.5	-0 ± 0.5	-2.5 ± 1	1 ± 0.5	0.5 ± 0.5	3.5 ± 1.5	1 ± 1	0.5± 0.5	6.5 ± 1
1,1.16 p-.5t	phase (degree)	-4 ± 14	0 ± 12	-21 ± 11	19 ± 10	7 ± 7	30 ± 12	20 ± 17	8 ± 10	53 ± 16
P min. O max.	phase (kyr)	-0 ± 0.5	0 ± 0.5	-2.5 ± 1	1 ± 0.5	0.5± 0.5	3.5 ± 1.5	1 ± 1	0.5± 0.5	6 ± 1

Table 4, Phase lags/leads of the Monte dei Corvi and Ceara Rise color data calculated using only the highest coherencies of the La2004$_{(1,1.135)}$ p.-5t and the La2004$_{(1,1.16)}$ p.-5t. Negative values indicated phase lead and positive values indicate a phase lag with the orbital solution.

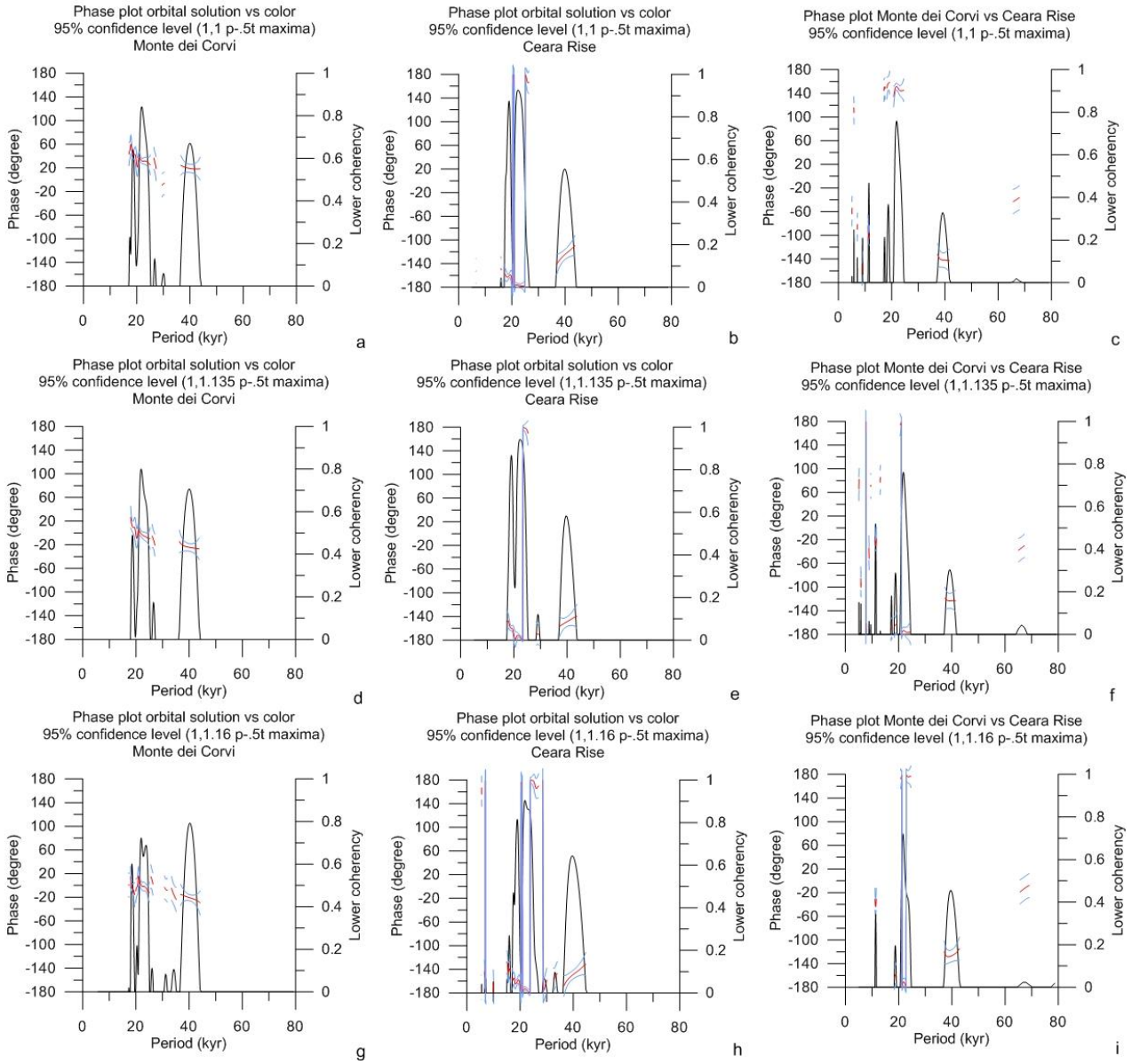

Figure 10, Phase plots of the Monte dei Corvi and Ceara Rise color data. A,d,g, Monte dei Corvi color data is plotted vs. La2004$_{(1,1)}$ p-.5t maxima, La2004$_{(1,1.135)}$ p-.5t maxima) and the La2004$_{(1,1.16)}$ p-.5t maxima. B,e,h, Ceara Rise color data is plotted vs. the tree solutions. C,f,i, cross-spectral comparison of the color records from the Monte dei Corvi and Ceara Rise using the tree solutions. Black line indicates lower coherency, red line indicates phase, blue lines indicate upper and lower phase. Negative values indicated phase lead and positive values indicate a phase lag with the orbital solution.

To get a better insight in the phase relations, a cross-spectral comparison was also made between the color records from Monte dei Corvi and Ceara Rise. At Ceara Rise however, the darker sediments, which are the reddish terrigenous clays and quartz, transported from the Amazon and other rivers, are probably related to precession maxima and obliquity minima (Tiedemann and Franz, 1997). So for Ceara Rise magnetic susceptibility maxima and the color (L*D65) *minima* are tuned to La2004$_{(1,1.135)}$ p-.5t and La2004$_{(1,1.16)}$ p-.5t *maxima*.

This results in the anti-phase relations between the two Sites that can be seen in Figure 10. For comparison however, Table 4 also shows the results of Ceara Rise color data but here the phases are recalculated for tuning L*D65 minima (darker layers) to precession minima and obliquity maxima (like the sapropels of Monte dei Corvi). These results are shown in Table 4.

7. Discussion

7.1 Age model

After making the phase plots (appendix 1 and Fig. 9), the magnetic susceptibility in the first and third age model revealed a roughly out of phase relation in the obliquity band with La2004$_{(1,1)}$ p-.5t and La2004$_{(1,1.135)}$ p-.5t minima, and thus with obliquity maxima. Tiedemann and Franz (1997) however, argued that glacial periods are linked to increased supply of terrigenous siliciclastics during low sea level stands when the Amazon River crossed the emerged shelf and discharged sediments directly into the Atlantic. This would result in high magnetic susceptibility values during colder periods (obliquity minima) and an anti-phase relation with insolation. If this is true, it means that age model 1 and 3 can only be correct if the magnetic susceptibility signal comes from a different source resulting in an in-phase relation with insolation. Age models 2, 4 and 5 do show the approximately anti-phase relation between the magnetic susceptibility and insolation and an in-phase relation between the magnetic susceptibility and the La2004 target curves. However, when using La2004$_{(1,1)}$ p-.5t maxima, a relatively large phase lag of ± 43 degree/5 kyr at the obliquity band is found. In case of the sapropels at Monte dei Corvi, which are linked to maximum African monsoon and supposedly reveal a direct response to all orbital parameters, this result would be unexpected, but at the Ceara Rise magnetic susceptibility and benthic foraminiferal $\delta^{18}O$ records could reflect a dominant obliquity control on glacial cyclicity, resulting in a lag. The interval from 9 to 10 Ma, occurs in a 2.4 Myr eccentricity minimum, coinciding with a relative increase in obliquity variability/influence. In this case heavier $\delta^{18}O$ values modulated by obliquity could indicate glacials (e.g. Holbourn et al., 2007). However, assuming that magnetic susceptibility does not come from a different source area, the relatively large (± 43 degree) phase lag of magnetic susceptibility relative to obliquity and the tuning results of the Monte dei Corvi, it is clear that the parameters for tidal dissipation and dynamical ellipticity have to be modified (Pälike and Shackleton, 2000) and that La2004$_{(1,1)}$ p-.5t is not the correct solution to analyze Ceara Rise data. In the following phase plots, the tuning to this solution is only plotted for comparison, but no interpretation of the leads/lags is given. Also the roughly anti-phase relation with the p-.5t target curves (age models 1 and 3), are considered less likely as this could only be true if there is a different source area for the magnetic susceptibility the Amazon sediment behavior changed. This is also the reason why magnetic susceptibility maxima are not tuned to La2004$_{(1,1.16)}$ p-.5t minima and why Figures 8, 9 and 10 only contain the plots for the

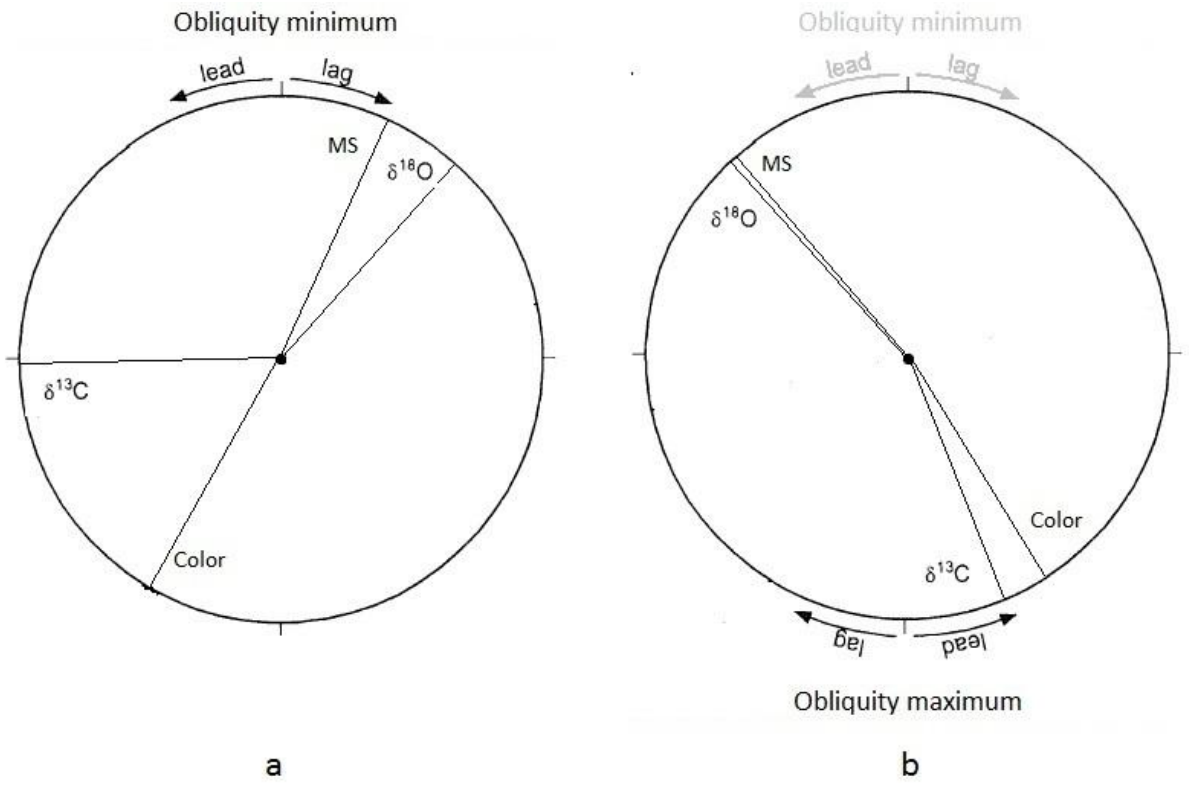

Figure 11. Phase relationships between time series of MS (magnetic susceptibility), color, benthic $\delta^{13}C$ and $\delta^{18}O$ maxima. a; Phases in degree calculated using the tuning to La2004$_{(1,1.135)}$ p-.5t maxima. b: Phase in degree calculated using the tuning to La2004$_{(1,1.35)}$ p-.5t minima.

tuning to La2004$_{(1,1.135)}$ p-.5t and La2004$_{(1,1.16)}$ p-.5t maxima.

Looking at the results in Table 3 and appendix 1i-l, it can be seen that for Ceara Rise magnetic susceptibility is approximately in anti-phase and the color data in-phase with the La2004$_{(1,1.135)}$ solution (tuning to p-0.5t minima). The benthic $\delta^{18}O$ data shows a ± 143 degree lag for the 23 kyr precession cycle and a ± 171 degree lag for the 19 kyr cycle. The coherency for 19 kyr is low and the phase difference is probably caused by the tuning to the precession cycle. For benthic $\delta^{18}O$, the obliquity related component reveals a ± 137 degree lag, corresponding to approximately 15 kyr. The benthic $\delta^{13}C$ data of the Ceara Rise shows, when using the tuning to the La2004$_{(1,1.135)}$ p-.5t minima, no 19 kyr precession cycle, a ± 113 degree lag for 23 kyr precession and a ± 22 degree lead for obliquity (Fig. 11).

When tuning the Ceara Rise data to the La2004$_{(1,1.135)}$ p-.5t maxima, the magnetic susceptibility is approximately in-phase and the color data in anti-phase (Table 3 and Fig.9). Benthic $\delta^{18}O$ shows an in-phase relation for 23 kyr precession, but a ± 40 degree lead for 19 kyr precession, probably also caused by the tuning to the precession cycle. For benthic $\delta^{18}O$ the obliquity cycle indicates a ± 36 degree lag to obliquity, corresponding to approximately 4 kyr. The benthic $\delta^{13}C$ data of the Ceara Rise shows, when using the tuning to the La2004$_{(1,1.135)}$ p-.5t maxima, no 19 kyr precession cycle, a ± 50 degree lead for 23 kyr precession and a ± 92 degree lead for obliquity (Fig. 11).

When tuning the Ceara Rise data to the La2004$_{(1,1.16)}$ p-.5t maxima it can be seen that magnetic susceptibility is also approximately in-phase and the color data in anti-phase (Table 3 and Fig.9). The benthic $\delta^{18}O$ data shows again an in-phase relation for the 23 kyr precession cycle but no 19 kyr precession cycle is found. This is probably caused by the 95% confidence level and it probably will be present using a lower confidence level. Benthic $\delta^{18}O$, the obliquity

cycle indicates a ± 18 degree lag to the solution, corresponding to approximately 2 kyr. The benthic $\delta^{13}C$ data of the Ceara Rise shows, when using the tuning to the $La2004_{(1,1.16)}$ p-.5t maxima, no 19 kyr precession cycle, a ± 28 degree lead for the 23 kyr precession cycle and a ± 107 degree lead for obliquity.

When comparing the magnetic susceptibility and the $\delta^{18}O$ data it can be seen that the difference in-phase is relatively small, so the approximately in-phase relation between these records, already noticed in the raw data, is correct.

To see which tuning is the best, Figure 11 shows the phase diagrams for the tuning to $La2004_{(1,1.135)}$ p-.5t maxima and minima. As explained earlier, the Ceara Rise benthic $\delta^{18}O$ record supposedly reflects a dominant obliquity control on glacial cyclicity. Ice growth occurs in-phase with obliquity minima (insolation minima) and during cooling, $\delta^{18}O$ values of the water will become heavier because the $\delta^{16}O$ is preferentially taken up in the ice (Lourens et al, 2010). However, it takes time to buildup the icecap, so in case of glacial cyclicity $\delta^{18}O$ maxima will lag obliquity minima. This is indeed shown in Figure 11a where based on the tuning of magnetic susceptibility maxima to $La2004_{(1,1.135)}$ p-.5t maxima (age model 4) where benthic $\delta^{18}O$ maxima lag obliquity minima by 36 degree. It can also be seen that the magnetic susceptibility maxima lag obliquity minima by 22 degree. This is in agreement with Tiedemann and Franz (1997), who argued that glacial periods are linked to increased supply of terrigenous siliciclastics during sea level low stands when the Amazon River crossed the emerged shelf and discharged sediments directly into the Atlantic. This would result in high magnetic susceptibility values during colder periods (obliquity minima). In case of tuning to $La2004_{(1,1.135)}$ p-.5t minima (Fig. 11b, shown in light grey), benthic $\delta^{18}O$ and magnetic susceptibility lead obliquity minima, which would not be correct. However, Houlbourn et al. (2007), stated that middle Miocene climate response was not solely coupled to changing high-latitude insolation and that additional interaction and/or feedback mechanisms also played a role.

In Tables 3 and 4 it can be observed that the age models based on the tuning to $La2004_{(1,1.16)}$ p-.5t maxima give almost the same results as tuning to $La2004_{(1,1.135)}$ p-.5t maxima. So it can be concluded that in the interval from 9 to 10 Ma, slight changes in the tidal dissipation parameter has little effect on the determination of the phase relation. Previous work of Zeeden et al. (in prep.) concluded that Monte dei Corvi, also used in this study, shows the best fit when tuned to $La2004_{(1,1.135)}$ p-.5t. Because also in this study the tuning to $La2004_{(1,1.135)}$ p-.5t maxima gave the most reasonable results for the phase relations at Ceara Rise, the results of tuning to $La2004_{(1,1.135)}$ p-.5t maxima are considered as most reliable. However, looking back at Figure 6 it seems that there is an error in the tuning of the Ceara Rise data in the first 3 meter. This will probably not give very different results for the Ceara Rise phase relations and the comparison with the Monte dei Corvi. However, this tuning error has to be solved to be certain that the tuning to $La2004_{(1,1.135)}$ p-.5t maxima gives the best fit, so more research has to be performed.

7.2 Phase difference

Looking at Table 4 it can be seen that the Monte dei Corvi color data shows a ± 24 degree lead for obliquity with the $La2004_{(1,1.135)}$ p-.5t, whereas the Ceara Rise color data shows a ± 30 degree lag at the obliquity cycle. The cross-spectral comparison of these two obliquity phases results in a ± 57 degree phase difference, corresponding to ± 6.5 kyr. During the Miocene the water

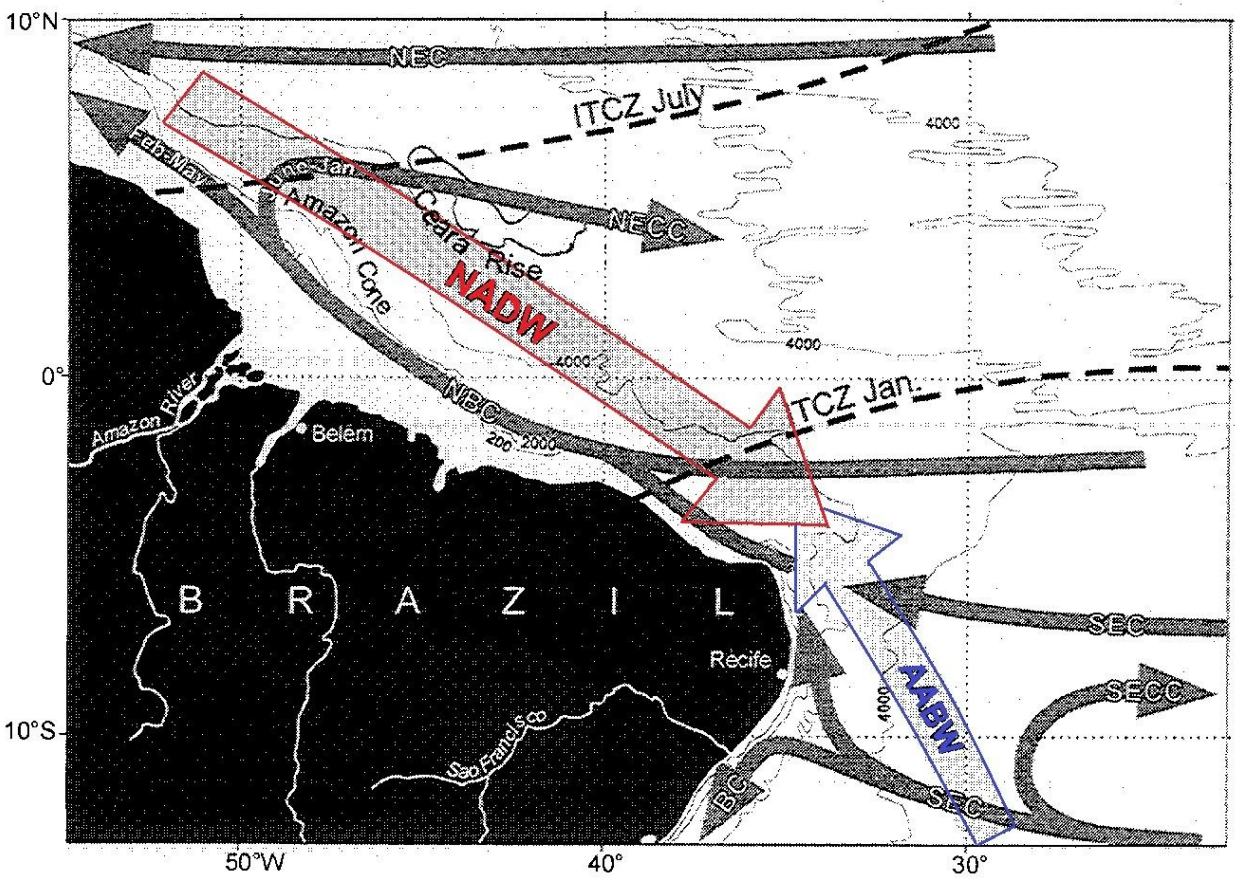

Figure 12, Figure showing the bathymetry, surface and deep water circulation, and seasonal positions of the Intertropical Convergence Zone (ITCZ). Surface water currents: SEC, South Equatorial Current; NBC North Brazil Current; NECC, North Equatorial Counter Current; SECC, South equatorial counter current; BC, Brazil Current. Deep water currents: AABW (blue), Antarctic Bottom water; NADW (red), Noth Atlantic Deep Water. Modified from Rühlemann et al., 2001.

circulation patterns in the Atlantic undertook much change. In the earliest Miocene the deep water system was dominated by Southern Component Water (SCW). During the early Miocene deep water circulation patterns were developed consisting of three independent water masses, two of which were relatively warm and saline (Tethyan water) (Woodruff and Savin, 1989) and the Northern Component Water (NCW) (Wright et al., 1992). These water masses supplemented the SCW production between 19 and 16 Ma. During the middle Miocene the production of the two warm water masses diminished and the production of the NCW and Tethyan waters was reduced, leaving the SCW as dominant deepwater mass ventilating the deep oceans (Wright and Miller, 1993). Several studies of the Miocene deepwater circulation patterns concluded that at about 12.5 Ma the NCW production was renewed and reached near-modern deep water circulation patterns during the late Miocene (Woodruff and Savin, 1989; Wright et al., 1992; Wright and Miller ,1993).

The ± 30 degree obliquity lag indicates that at the Ceara Rise the response to precession is independent of the response to obliquity (glacial cyclicity) (Pfuhl and Shackleton, 2004; Holbourn et al., 2007)) while at Monte dei Corvi both cycles are dependently as they affect the same part of the climate system (direct response African of Monsoon). At low latitudes precession has more influence, whereas at high latitudes obliquity is of greater influence (e.g. Berger and Tricot, 1986). Therefore, the precessional signal at the Ceara Rise is probably local and recorded in the overlying waters (surface waters and NADW), while the deep water masses formed at high southern latitudes

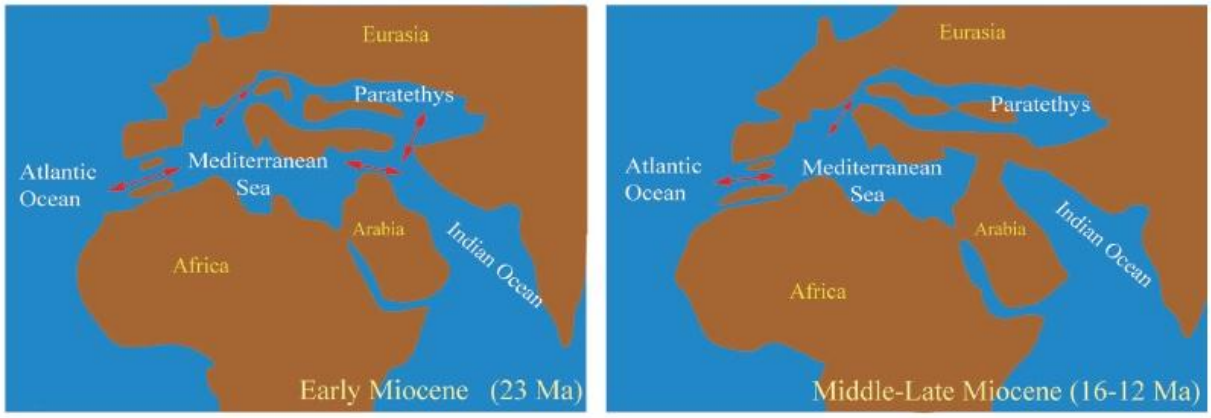

Figure 13, Reconstructions of the land sea distribution during the Miocene. Left; Mediterranean Sea and Paratethys still had open gateways towards Indian Ocean. Right; Mediterranean Sea and Paratethys after closure gateways Indian Ocean. Modified from Karami, 2011.

(AABW) contain the obliquity signal (Pfuhl and Shackleton, 2004).

Figure 12 shows the modern circulation patterns of the western Atlantic. Ceara Rise Site 926 is drilled at approximately 3600 meter and is recently bathed in NADW. The NADW now occupies the depth interval between 2000 and 4000 meter and it is underlying by the AABW. The gradients in temperature, salinity, nutrient concentrations, and corrosiveness of the water with respect to calcium carbonate mark the mixing zone between the NADW and the AABW (Bickert et al.,1997). Tiedemann and Franz (1997) suggested that during the middle Pliocene in response to vertical movements of the mixing zone in the equatorial West Atlantic, carbonate preservation could be linked to high-latitude, climatically induced, changes in deep-water circulation that led to a cyclic shoaling and deepening of the lysocline at a 41 kyr rhythm. Their results indicated that maxima in carbonate dissolution at 4356m water depth lead maxima ice volume by 8 kyr in the obliquity band and suggest an early response to climate change in the Southern Ocean. They also concluded that this phasing decreased toward shallower water depths returning to the in-phase relation with changes in global ice volume.

The ± 30 degree lag for the obliquity cycle found in this study also indicate that between 9 and 10 Ma the obliquity signal recorded in the deep water masses entering Ceara Rise is probably related to a delayed response with climate change in the southern Ocean.

During the Miocene the water circulation patterns in the Mediterranean Sea also undertook much change (Fig. 13). In the early Miocene and part of the middle Miocene the Mediterranean Sea was still connected to the Paratethys (now the Black Sea and Caspian Sea) and both the Atlantic and Indian Ocean. During the middle-late Miocene the gateways to the Indian Ocean were closed (Meulenkamp and Sissingh, 2003; Karami, 2011; Karami et al., 2011). Between 9 and 10 Ma the Monte dei Corvi site was only influenced by shallow water flowing in the Mediterranean Sea from the Atlantic Ocean and the Paratethys, so no deep water currents from high latitudes, which may carry an obliquity signal, when entering the Mediterranean Sea. As explained before sapropels are directly linked to maximum African Monsoon and climate modeling results show an in-phase behavior/direct response of the African monsoon relative to astronomical forcing by both the precession and obliquity

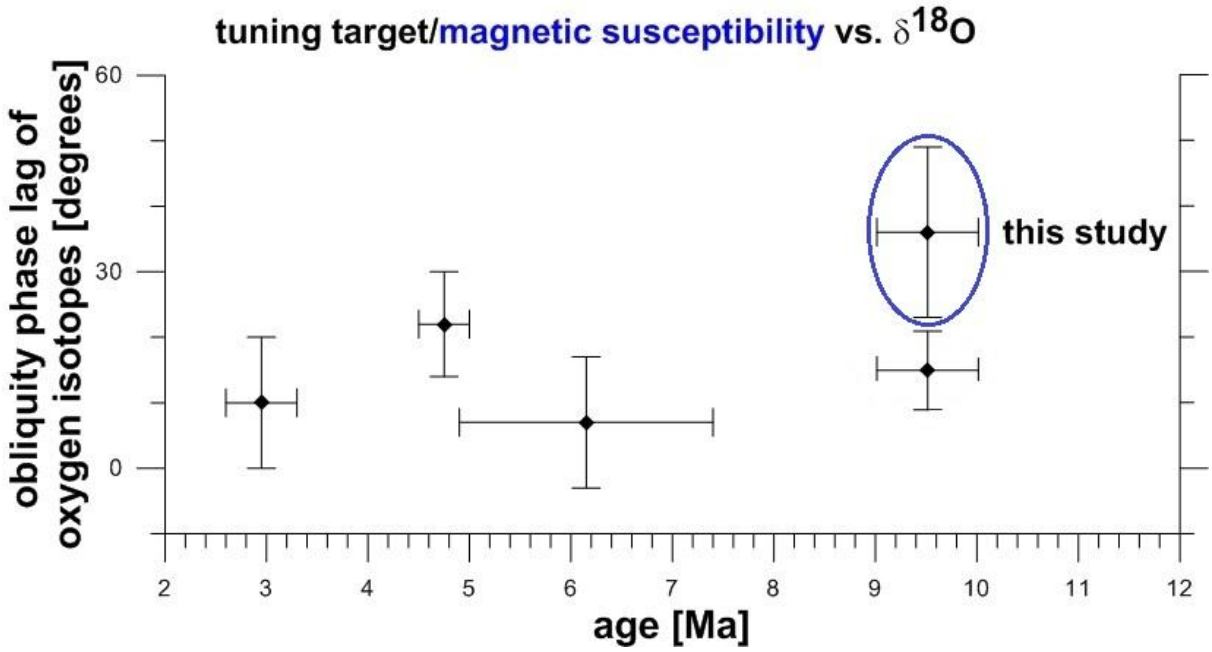

Figure 14, Phases of oxygen isotope data relative to the magnetic susceptibility and tuning targets from this study around 9-10 Ma) and other studies from the equatorial Atlantic Ceara Rise. Some data from Shackleton and Crowhurst (1997) and Shackleton and Hall (1997) were not included due to tuning issues in their Miocene record. Data of Pälike et al. (2006) are also not included because they used the spliced and stacked susceptibility and reflectance ('SusRe'') record. From poster Zeeden et al., 2012.

cycles, resulting in the roughly in-phase relation (24 ± 10 degrees lead) of obliquity.

So when comparing the phase relations of the Monte dei Corvi and Ceara Rise, the Ceara Rise color data will lag the Monte dei Corvi data by ± 57 degree at the obliquity band. This lag is caused by the deep water currents entering the Ceara Rise which contain the delayed obliquity signal. The Monte dei Corvi is not influenced by these deep water currents.

7.3 Comparison phases over time

Tiedemann and Franz (1997) generated an orbitally tuned time scale for Ceara Rise for the time interval from 3.3 to 2.6 Ma and 5 to 4.5 Ma. They tuned the magnetic susceptibility maxima to $La90_{(1,1)}$ 65° northern hemisphere insolation minima, as indicated by their benthic $\delta^{18}O$ records from Site 926 (magnetic susceptibility maxima occurred during cold stages). They assumed no phase difference between magnetic susceptibility and northern hemisphere insolation, which might be oversimplified but according to them this would result in a minor error of the tuned time scale. Only their results of the cross-spectral analyses reveal that the negative $\delta^{18}O$ fluctuations tend to lag northern hemisphere summer insolation by 1 ± 1 kyr (middle Pliocene) and 2.5 ± 1 kyr (early Pliocene) in the obliquity band. The obliquity related $\delta^{13}C$ maxima (indicative of deep water ventilation maxima) lag ice-volume maxima by about 4 ± 2 kyr. The AABW, which is the southern deep water source at Ceara Rise, transferred a ± 8 kyr earlier dissolution signal of the Southern Ocean into the equatorial Atlantic during ice growth than the intermediate NADW.

Shackleton and Crowhurst (1997) generated an orbitally tuned time scale for the interval from 4.9 to 7.4 and 10.97 to 13.2 Ma, correlating susceptibility maxima to $La90_{(1,1)}$ 65° Northern Hemisphere insolation minima. They show that negative benthic $\delta^{18}O$ have zero phase lag with respect to high-latitude insolation at the main obliquity frequency. In the interval from 4.9 to 7.4 Ma the phase remains rather constant, but in the older

interval it is more variable. In the interval from 4.7 to 7.4 Ma, the obliquity component in $\delta^{18}O$ lags insolation by ± 7 degree. At the interval from 10.97 to 13.2 Ma this component lags with insolation ± 141 degree. This large phase lag is incorrect because of the stratigraphic and tuning problems they encountered in this interval.

Shackleton and Hall (1997) assigned ages to their time scale using the ages of Shackleton and Crowhurst (1997). Their results indicate that between 5 and 14 Ma the positive $\delta^{13}C$ is lagging high latitude insolation by about 90° (10 kyr).

Between 17.86 and 26.5 Ma, Pälike et al. (2006) re-adjusted the astronomical age calibration of ODP leg 154 to the newer astronomical solution, La2004 using current day values for tidal dissipation and dynamical ellipticity. They also multiplied the stable isotope series with -1, aligning $\delta^{18}O$ maxima with temperature minima/ice volume maxima. Cross-spectral analysis between the ETP curve and the negative stable isotope series resulted in an obliquity lag of about 31° for the benthic $\delta^{18}O$. The $\delta^{13}C$ showed an almost 180° out of phase relation with the oxygen isotope data.

As mentioned before in this study, when tuning the Ceara Rise data to $La2004_{(1,1.135)}$ p-.5t maxima, $\delta^{18}O$ lags obliquity by ± 36 degree. However when looking at the $\delta^{18}O$ data relative to the magnetic susceptibility data, $\delta^{18}O$ lags obliquity with ± 14 degree. Figure 14 shows the phase of the different studies and this study over time. It can be seen that at Ceara Rise the obliquity phase between the magnetic susceptibility and the benthic $\delta^{18}O$ record, when assuming that the magnetic susceptibility responds directly to orbital forcing, has stayed relatively constant over time. However, at Ceara Rise the magnetic susceptibility is not in-phase with orbital forcing at the obliquity band, caused by glacial cyclicity and the results indicated a ± 36 degree lag for the $\delta^{18}O$ record. This indicates that the phase of the magnetic susceptibility as tuning target appears to have changed over time and shows that more research has to be carried out about this change in-phase over time. For a better comparison, also the different age models should be updated to the same age model that shows the best fit and include the correct values for the tidal dissipation and dynamical ellipticity in the astronomical solution.

8. Conclusions

1. For Ceara Rise the tuning to $La2004_{(1,1.135)}$ p-.5t maxima gives the most reasonable phase relations.
2. Slightly changing the tidal dissipation parameter does not have much effect on the determination of phase relations between 9 and 10 Ma.
3. The ± 22 degrees lag between magnetic susceptibility and obliquity based on the tuning to $La2004_{(1,1.135)}$ p-.5t maxima is related to an indirect response to astronomical forcing, which is related to glacial cyclicity, at Ceara Rise.
4. The Ceara Rise color data lag the Monte dei Corvi data by ± 57 degree in the obliquity band. This lag is probably caused by deep water currents from the southern ocean containing a delayed obliquity signal related to glacial cyclicity.
5. The phase between the magnetic susceptibility and the benthic oxygen isotope record has stayed relatively constant over time. However, the phase of the magnetic susceptibility as tuning target may have changed over time.

Acknowledgements

I would like to thank Christian Zeeden and Frits Hilgen for helping me with everything during the sample preparation, writing, taking me on the field trip to the Monte dei Corvi section and for the good times we had there. I am also grateful for the help of the people at the MARUM, Center for marine environmental sciences, University of Bremen, for cooperation when taking the samples from the Ceara Rise cores. I would also like to thank Dominika Kasjaniuk and Arnold van Dijk for the technical support and last but not least I would like to thank Agnes van Loevezijn, Luuk Thijssen and my parents and sister for their support.

References

Balsam, W.L., Otto - Bliesner, B.L., Deaton, B.C. 1995 Modern and last glacial maximum eolian sedimentation patterns in the Atlantic Ocean interpreted from sediment iron oxide content. *Paleoceanography*, volume 10, pp. 493-508.

Berger, A.L., Tricot, C. 1986 Global climatic changes and the theory of paleoclimates. In: *Cazenace, A. (Ed.), Earth rotation: Solved and unsolved problems*. Reidel Publishing Company, Dordrecht, pp. 111-129.

Bickert, T., Curry, W.B., Wefer, G. 1997 Late pliocene to Holocene (2.6-0 Ma) western equatorial Atlantic Deep-water circulation: interences from benthic stable isotopes. *Proceedings of the Ocean Drilling Program*, *Scientific results*, volume 154, pp. 239-254.

Harris, S.E., Mix, A.C., King, T. 1997 Biogenic and terrigenous sedimentation at Ceara Rise, western tropical Atlantic, supports Pliocene-Pleistocene deep-water linkage between hemispheres. *Proceedings of the Ocean Drilling Program*, *Scientific results*, volume 154, pp. 331-345.

Hilgen F.J., 1991 Extension of the astronomically calibrated (polarity) time scale to the Miocene/Pliocene boundary. *Earth Planet. Science Letters, volume* 107, pp. 349-368.

Holbourn, A., Kuhnt, W., Schulz, M., Flores, J-A., Andersen, N. 2007 Orbitally-paced climate evolution during the middle Miocene `Monterey´ carbon-isotope excursion. *Earth and Planetary Science Letters*, volume 261, pp. 534-550.

Hüsing, S.J., Hilgen, F.J., Abdul Aziz, H., Krijgsman, W. 2007 Completing Neogene geological time scale between 8.5 and 12.5 Ma. *Earth and Planetary Science Letters*, volume 253, pp. 340-358.

Karami, M.P., 2011 Paleoceanography of the Miocene Mediterranean Sea and Paratethys: Regional ocean modeling of the response to closure of the Thetys Seaway. Proefschrift, *Utrecht University, Faculty of Geosciences, Department of Earth Sciences*.

Karami, M.P., Leeuw de, A., Krijgsman, W., Meijer, P.Th., Wortel, M.J.R. 2011 The role of gateways in the evolution of temperature and salinity of semi-enclosed basins: An oceanic box model for the Miocene Mediterranean Sea and Paratethys. *Elsevier*, volume 79, pp. 73-88.

Laskar, J., Joutel, F., Boudin, F. 1993 Orbital, precession and insolation quantities for the Earth from -20 Myr to +10 Myr Asrton. *Astrophysical*, volume 270, pp. 522-533.

Laskar, J., Robutel, P., Joutel, F., Gastineau, M., Correia, A., Levard, B., 2004 A long term numerical solution for the insolation quantities of the Earth. *Astronomy and Astrophysics*, volume 428, p.p. 261-285.

Lourens, L.J., Becker, J., Bintanja, R., Hilgen, F.J., Teunter, E., van de Wal, R.S.W., Ziegler, M. 2010 Linear and non-linear response of late Neogene glacial cycles to obliquity forcing and implications for the Milankovitch theory. *Elsevier*, Volume 29, issues 1-2, pp. 353-365.

Meulenkamp, J.E. and Sissingh, W., 2003 Tertiary palaeogeography and tectonostratigraphic evolution of the Northern and Southern Peri-Tethys platforms and the intermediate domains of the African-Eurasian convergent plate boundary zone. *Elsevier*, volume 196, pp. 209-228.

Pälike, H., Frazier, J., Zachos, J. 2006 Extended orbitally forced palaeoclimatic records from the equatorial Atlantic Ceara Rise. *Quaternary Science Reviews,* volume 25, pp. 3138-3149.

Pälike, H, Shackleton, N.J., 2000 Constrains on astronomical parameters from the geological record for the last 25 Myr *Earth and Planetary Science Letters*, volume 182, pp. 1-14.

Pfuhl, H.A., Shackleton, N.J. 2004 Two proximal, high-resolution records of foraminiferal fragmentation and their implications for changes in dissolution. *Elsevier, Deep-Sea Research I*, volume 51, pp. 809-832.

Rühlemann, C., Diekmann, B., Mulitza, S., Frank, M. 2001

Late Quarternary changes of western equatorial Atlantic surface circulation and Amazone lowland climate recorded in Ceara Rise deep-sea sediments. *Paleoceanography*, volume 16, pp. 293-305.

Shackleton, N.J. and Crowhurst, S. 1997 Sediment fluxes based on an orbitally tuned time scale 5 Ma to 14 Ma, site 926. *Proceedings of the Ocean Drilling Program*, *Scientific results*, volume 154.

Shackleton, N.J., Crowhurst, S.J., Weedon, G.P., Laskar, J. 1999 Astronomical calibration of Oligocene-Miocene time. *Philosophical Transactions: Mathematical, Physical and Engineering Science*, volume 357, pp. 1907-1929. The Royal Society.

Teunter, E., Weber, S.L., Hilgen, F.J., Lourens, L.J., Ganopolski, A., 2005 Simulation of climate phase lags in response to precession and obliquity forcing and the role of vegetation. *Climate Dynamics*, volume 24, pp. 279-295.

Tiedemann, R., Franz, S.O. 1997 Deep-water circulation, chemistry, and terrigenous sediment supply in the equatorial atlantic during the Pliocene, 3.3-2.6 Ma and 5-4.5 Ma. *Proceedings of the Ocean Drilling Program*, *Scientific results*, volume 154, pp. 299-318.

Woodruff, F., Savin, S.M., 1989 Miocene deepwater oceanography, *Paleoceanography,* volume 4, pp. 87-140.

Wright, J.D., Miller, K.G. 1993 Southern ocean influences on late Eocene to Miocene deepwater circulation. *The Antarctic paleoenvironment: A perspective on global change Antarctic research series*, volume 60, pp. 1-25.

Wright, J.D., Miller, K.G., Fairbanks, R.G., 1992 Early and middle Miocene sTable isotopes: implications for deepwater circulation and climate. *Paleoceanography*, volume 7 (3), pp. 357-389.

Zeeden, C., de Jonge, J.A.J., Hilgen, F.J., Lourens, L.J., 2012 Phase relations between orbital forcing and terrestrial response in the equatorial Atlantic over the last 10 Ma. *Utrecht University*, poster.

Zeeden, Z., Hilgen, F.J., Lourens, L.J., Hüsing, S., 2012 The Neogene astronomical tuned (polarity) timescale between 5 and 14 Ma revisited. *Utrecht University*, poster.

Ziegler, M., Teunter, E., Lourens, L.J., 2010 The precession phase of the boreal summer monsoon as viewed from the eastern Mediterranean (ODP Site 968). *Elsevier*, volume 29, pp. 1481-1490.

Appendix

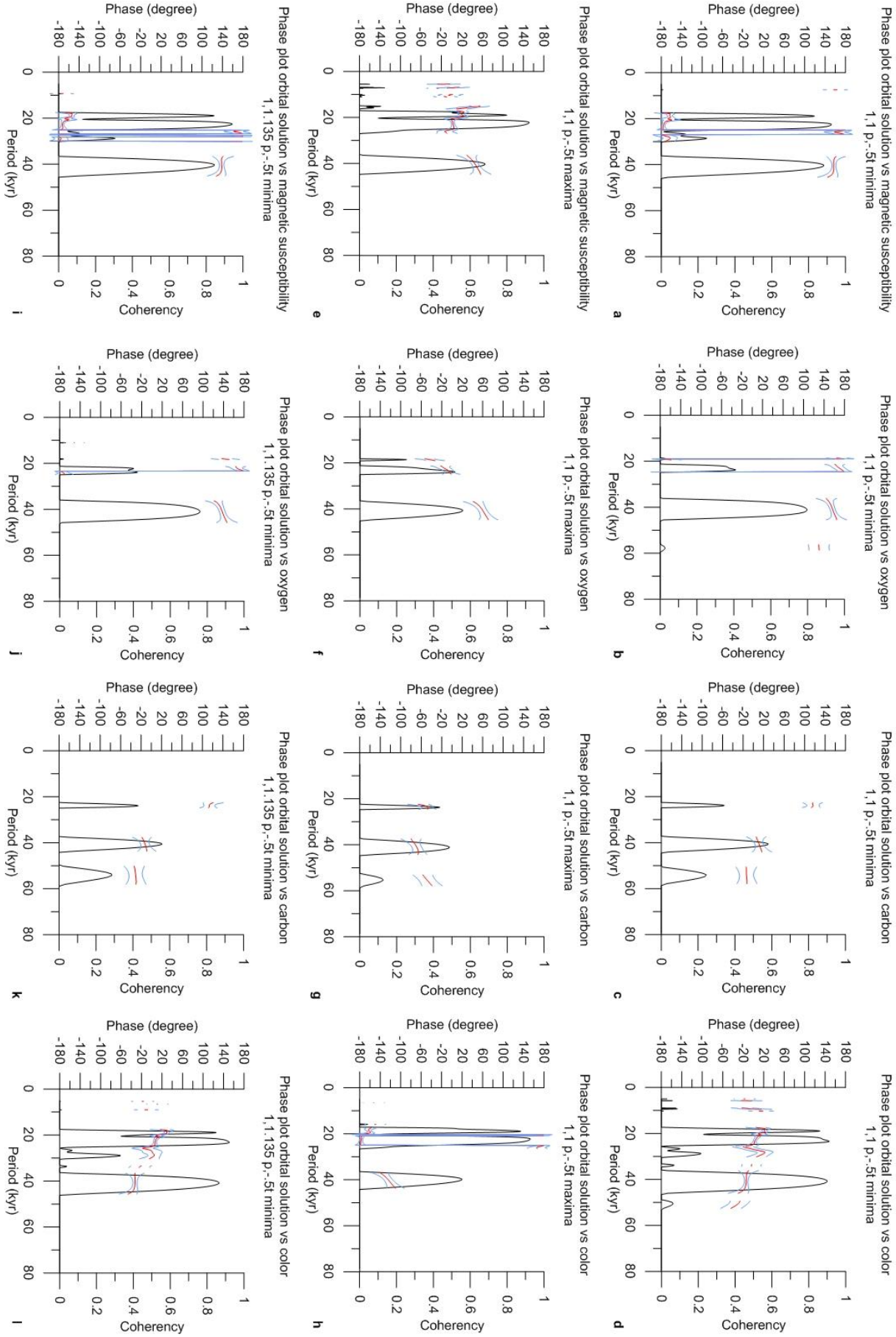

Appendix 1, Phase plots of magnetic susceptibility, sTable isotope and color data established with different age models. a-d . Phase plots of MS, sTable isotope data and color data versus the orbital solution using the first age model (La2004$_{(1,1)}$ p-5t minima). e-h. Phase plots of MS, sTable isotope data and color data versus the orbital solution using the second age model (La2004$_{(1,1)}$ p-5t maxima). i-l. Phase plots of MS, sTable isotope data and color data versus the orbital solution using the third age model (La2004$_{(1.1.135)}$ p-5t minima).

Expedition	Site	Hole	Sample code	TOP_depth	BOTTOM_depth	MBSF_TOP	MCD_TOP	Composite depth	(1,1.1 p-.5t maxima)	(1,1.135 p-.5t minima)	(1,1.16 p-.5t maxima)	Xsp (m³/kg)	Average L*(D65)	Fraction measured*	Wuellestorfi amount **	Mundulus amount **	d13C	d18O
154	926	A	JA1	98	100	204.48	228.54	0.00	#N/A	#N/A	#N/A	5.43E-08	69.63	B		5	1.32	2.32
154	926	A	JA2	102	104	204.52	228.58	0.04	#N/A	#N/A	#N/A	5.25E-08	69.28	B	1	1	1.45	2.31
154	926	A	JA3	106	108	204.56	228.62	0.08	#N/A	#N/A	#N/A	5.18E-08	69.60	B		3	1.25	2.26
154	926	A	JA4	110	112	204.60	228.66	0.12	#N/A	#N/A	#N/A	5.46E-08	68.62	B		3	0.73	2.32
154	926	A	JA5	114	116	204.64	228.70	0.16	#N/A	#N/A	#N/A	6.42E-08	65.27	B	1	1	0.88	2.28
154	926	A	JA6	118	120	204.68	228.74	0.20	#N/A	#N/A	#N/A	6.79E-08	64.27	B		4	1.10	2.05
154	926	A	JA7	122	124	204.72	228.78	0.24	#N/A	#N/A	#N/A	7.46E-08	59.49	B	5		1.21	1.83
154	926	A	JA8	126	128	204.76	228.82	0.28	#N/A	#N/A	#N/A	9.02E-08	55.53	B	2		1.12	2.29
154	926	A	JA9	130	132	204.80	228.86	0.32	#N/A	#N/A	#N/A	9.35E-08	56.49	B		2	1.10	1.71
154	926	A	JA10	134	136	204.84	228.90	0.36	9026.00	9035	9024.00	9.62E-08	55.25	B		3	1.13	2.46
154	926	A	JA11	138	140	204.88	228.94	0.40	9028.71	9037.588	9026.59	9.96E-08	56.45	A		2	1.39	2.59
154	926	A	JA12	142	144	204.92	228.98	0.44	9031.41	9040.176	9029.18	6.57E-08	64.89	C			0.91	2.45
154	926	A	JA13	146	148	204.96	229.02	0.48	9034.12	9042.765	9031.76	5.57E-08	67.32	B		1	0.90	2.11
154	926	A	JA15	0	2	205.00	229.06	0.52	9036.82	9045.353	9034.35	5.21E-08	70.54	B		1	1.19	2.42
154	926	A	JA16	4	6	205.04	229.10	0.56	9039.53	9047.941	9036.94	5.70E-08	65.72	B		2	1.28	2.25
154	926	A	JA17	8	10	205.08	229.14	0.60	9042.24	9050.529	9039.53	6.31E-08	67.49	B		5	1.26	2.19
154	926	A	JA18	12	14	205.12	229.18	0.64	9044.94	9053.118	9042.12	8.39E-08	61.34	B		1	1.23	2.28
154	926	A	JA19	16	18	205.16	229.22	0.68	9047.65	9055.706	9044.71	9.11E-08	57.43	B		5	1.27	2.30
154	926	A	JA20	20	22	205.20	229.26	0.72	9050.24	9058.294	9047.29	9.33E-08	57.39	B		3	1.35	2.26
154	926	A	JA21	24	26	205.24	229.30	0.76	9052.71	9060.882	9049.88	7.60E-08	64.83					
154	926	A	JA22	28	30	205.28	229.34	0.80	9055.18	9063.471	9052.47	6.35E-08	68.51	B		1	1.41	2.15
154	926	A	JA23	32	34	205.32	229.38	0.84	9057.65	9066.059	9055.06	6.23E-08	66.33	B	1	2	1.31	2.22
154	926	A	JA24	36	38	205.36	229.42	0.88	9060.12	9068.647	9057.65	7.18E-08	66.47	A			1.31	2.50
154	926	A	JA25	40	42	205.40	229.46	0.92	9062.59	9071.235	9060.24	7.04E-08	66.12					
154	926	A	JA26	44	46	205.44	229.50	0.96	9065.06	9073.824	9062.82	7.72E-08	63.65	B		2	1.26	2.22
154	926	A	JA27	48	50	205.48	229.54	1.00	9067.53	9076.412	9065.41	8.78E-08	56.76	B		2	1.19	2.15
154	926	A	JA28	52	54	205.52	229.58	1.04	9070.00	9079	9068.00	1.07E-07	54.23	B	3		1.45	2.47
154	926	A	JA29	56	58	205.56	229.62	1.08	9072.41	9081.462	9070.41	1.02E-07	54.30	B		4	1.09	2.55
154	926	A	JA30	60	62	205.60	229.66	1.12	9074.82	9083.923	9072.82	8.84E-08	60.21	B	3		1.23	2.52
154	926	A	JA31	64	66	205.64	229.70	1.16	9077.23	9086.385	9075.23	7.13E-08	66.30	B	2	2	1.48	2.54
154	926	A	JA32	68	70	205.68	229.74	1.20	9079.64	9088.846	9077.64	6.59E-08	66.41	B		5	1.39	2.57
154	926	A	JA33	72	74	205.72	229.78	1.24	9082.05	9091.308	9080.05	6.25E-08	67.79	B		1	1.48	2.33
154	926	A	JA38	76	78	205.76	229.82	1.28	9084.46	9093.769	9082.46	6.01E-08	67.99	B		1	1.25	2.47
154	926	A	JA34	80	82	205.80	229.86	1.32	9086.87	9096.231	9084.87	6.22E-08	69.16	B		3	0.84	2.57
154	926	A	JA35	84	86	205.84	229.90	1.36	9089.28	9098.692	9087.28	6.58E-08	67.29	B	1	2	1.39	2.49
154	926	A	JA36	88	90	205.88	229.94	1.40	9091.69	9101.154	9089.69	6.43E-08	66.01	B	1		1.49	2.60
154	926	A	JA37	92	94	205.92	229.98	1.44	9094.10	9103.615	9092.10	6.08E-08	67.41	B		3	1.27	2.55
154	926	A	JA39	96	98	205.96	230.02	1.48	9096.51	9106.077	9094.51	6.00E-08	66.18	B	7		1.40	2.61
154	926	A	JA40	100	102	206.00	230.06	1.52	9098.92	9108.538	9096.92	6.40E-08	67.74	B	5		1.40	2.39
154	926	A	JA41	104	106	206.04	230.10	1.56	9101.33	9111	9099.33	6.10E-08	65.98	A	1		1.42	2.39
154	926	A	JA42	108	110	206.08	230.14	1.60	9103.74	9113.462	9101.74	5.37E-08	68.53	B		2	1.41	2.51
154	926	A	JA43	112	114	206.12	230.18	1.64	9106.15	9115.923	9104.15	4.56E-08	70.21	B	2		1.44	2.38
154	926	A	JA44	116	118	206.16	230.22	1.68	9108.56	9118.385	9106.56	5.29E-08	68.40	A			1.36	2.36
154	926	A	JA45	120	122	206.20	230.26	1.72	9110.97	9120.846	9108.97	5.67E-08	67.29	B	1	2	1.35	2.28
154	926	A	JA46	124	126	206.24	230.30	1.76	9113.38	9123.308	9111.38	5.80E-08	68.97					
154	926	A	JA47	128	130	206.28	230.34	1.80	9115.79	9125.769	9113.79	6.80E-08	64.92					
154	926	A	JA48	132	134	206.32	230.38	1.84	9118.20	9128.15	9116.20	8.55E-08	60.52	B		1	1.22	2.53
154	926	A	JA49	136	138	206.36	230.42	1.88	9120.60	9130.45	9118.60	7.13E-08	66.24	B	4		1.39	2.26
154	926	A	JA50	140	142	206.40	230.46	1.92	9123.00	9132.75	9121.00	6.11E-08	70.28	B		2	1.26	2.24

154	926	A	JA51	144	146	206.44	230.50	1.96	9125.40	9135.05	9123.40	5.03E-08	69.41	B	1	1	1.34	2.27
154	926	A	JA52	148	150	206.48	230.54	2.00	9127.80	9137.35	9125.80	4.95E-08	71.17	B		1	0.90	2.22
154	926	A	JA53	0	2	206.50	230.56	2.02	9129.00	9138.5	9127.00	4.73E-08	70.15	B	1	2	1.28	2.26
154	926	A	JA54	4	6	206.54	230.60	2.06	9131.40	9140.8	9129.40	5.91E-08	68.19	B		4	1.22	2.27
154	926	A	JA55	8	10	206.58	230.64	2.10	9133.80	9143.1	9131.80	5.90E-08	67.97	B		4	1.27	2.32
154	926	A	JA56	12	14	206.62	230.68	2.14	9136.20	9145.4	9134.20	6.97E-08	64.74	A	1		1.28	2.41
154	926	A	JA57	16	18	206.66	230.72	2.18	9138.60	9147.7	9136.60	8.75E-08	58.77	B	1	1	1.50	2.33
154	926	A	JA58	20	22	206.70	230.76	2.22	9141.00	9150	9139.00	9.56E-08	57.69	B		2	1.18	2.42
154	926	A	JA59	24	26	206.74	230.80	2.26	9143.44	9152.333	9141.44	8.04E-08	58.22	B		2	1.14	2.52
154	926	A	JA60	28	30	206.78	230.84	2.30	9145.89	9154.667	9143.89	5.94E-08	68.34	B		2	1.33	2.35
154	926	A	JA61	32	34	206.82	230.88	2.34	9148.33	9157	9146.33	5.73E-08	69.15	B		2	1.38	2.24
154	926	A	JA62	36	38	206.86	230.92	2.38	9150.78	9159.333	9148.78	5.42E-08	70.28	B		3	1.27	2.27
154	926	A	JA63	40	42	206.90	230.96	2.42	9153.22	9161.667	9151.22	5.36E-08	67.53	B		1	1.24	2.19
154	926	A	JA64	44	46	206.94	231.00	2.46	9155.67	9164	9153.67	5.75E-08	64.75	B		3	1.32	2.37
154	926	A	JA65	48	50	206.98	231.04	2.50	9158.11	9166.333	9156.11	7.45E-08	64.36	B		2	1.17	2.51
154	926	A	JA66	52	54	207.02	231.08	2.54	9160.56	9168.667	9158.56	8.71E-08	61.25	B		3	1.32	2.49
154	926	A	JA67	56	58	207.06	231.12	2.58	9163.00	9171	9161.00	9.33E-08	58.61	B	1	1	1.25	2.35
154	926	A	JA68	60	62	207.10	231.16	2.62	9165.21	9173.316	9163.21	7.03E-08	69.55	B	1	2	1.42	2.43
154	926	A	JA69	64	68	207.14	231.20	2.66	9167.42	9175.632	9165.42	6.17E-08	68.41	B		2	1.44	2.25
154	926	A	JA70	68	70	207.18	231.24	2.70	9169.63	9177.947	9167.63	5.84E-08	69.55	B		1	1.40	2.52
154	926	A	JA71	72	74	207.22	231.28	2.74	9171.84	9180.263	9169.84	6.33E-08	66.54	B	1	2	1.41	2.34
154	926	A	JA72	76	78	207.26	231.32	2.78	9174.05	9182.579	9172.05	7.33E-08	67.58	B	1	1	1.41	2.24
154	926	A	JA73	80	82	207.30	231.36	2.82	9176.26	9184.895	9174.26	7.36E-08	67.83	B		1	1.23	2.47
154	926	A	JA74	84	86	207.34	231.40	2.86	9178.47	9187.211	9176.47	7.97E-08	64.07	B		4	1.21	2.59
154	926	A	JA75	88	90	207.38	231.44	2.90	9180.68	9189.526	9178.68	7.42E-08	64.56	B		3	1.27	2.51
154	926	A	JA76	92	94	207.42	231.48	2.94	9182.89	9191.842	9180.89	8.59E-08	59.73	B	1	2	1.14	2.70
154	926	A	JA77	96	98	207.46	231.52	2.98	9186.28	9194.531	9184.22	8.47E-08	61.11	B		4	1.23	2.64
154	926	A	JA78	100	102	207.50	231.56	3.02	9190.84	9197.594	9188.66	7.65E-08	62.40	B		1	1.12	2.53
154	926	A	JA79	104	106	207.54	231.60	3.06	9195.41	9200.656	9193.09	7.22E-08	63.19	B		1	1.10	2.35
154	926	A	JA80	108	110	207.58	231.64	3.10	9199.97	9203.719	9197.53	7.13E-08	64.32	B		2	1.35	2.61
154	926	A	JA81	112	114	207.62	231.68	3.14	9204.53	9206.781	9201.97	6.79E-08	66.59	B	3		1.45	2.44
154	926	A	JA82	116	118	207.66	231.72	3.18	9209.09	9209.844	9206.41	5.69E-08	70.81	B	1		1.39	2.34
154	926	A	JA83	120	122	207.70	231.76	3.22	9213.66	9212.906	9210.84	5.90E-08	69.53	B		3	1.28	2.46
154	926	A	JA84	124	126	207.74	231.80	3.26	9218.22	9215.969	9215.28	6.13E-08	67.10	B		1	1.33	2.38
154	926	A	JA85	128	130	207.78	231.84	3.30	9222.78	9219.031	9219.72	5.72E-08	67.97	B	1	2	1.21	2.39
154	926	A	JA86	132	134	207.82	231.88	3.34	9227.34	9222.094	9224.16	5.06E-08	70.31	B		1	1.19	2.38
154	926	A	JA87	136	138	207.86	231.92	3.38	9231.91	9225.156	9228.59	5.69E-08	68.63	B	4		1.41	2.39
154	926	A	JA88	140	142	207.90	231.96	3.42	9236.47	9228.219	9233.03	5.89E-08	64.63	B	1	2	1.27	2.43
154	926	A	JA89	144	146	207.94	232.00	3.46	9241.03	9231.281	9237.47	6.98E-08	61.05	B	2		1.37	2.31
154	926	A	JA90	148	150	207.98	232.04	3.50	9245.59	9234.344	9241.91	8.27E-08	59.18	B	3		1.28	2.31
154	926	A	JA91	0	2	208.00	232.06	3.52	9247.88	9235.875	9244.13	8.85E-08	58.29	A	1		1.19	2.53
154	926	A	JA92	4	6	208.04	232.10	3.56	9252.44	9238.938	9248.56	1.03E-07	54.85	B		1	1.08	2.50
154	926	A	JA93	8	10	208.08	232.14	3.60	9257.00	9242	9253.00	1.03E-07	55.51			1		
154	926	A	JA94	12	14	208.12	232.18	3.64	9259.56	9244.625	9255.56	9.68E-08	58.80	B	2		1.29	2.60
154	926	A	JA95	16	18	208.16	232.22	3.68	9262.13	9247.25	9258.13	6.63E-08	67.44	B		2	1.38	2.20
154	926	A	JA96	20	22	208.20	232.26	3.72	9264.69	9249.875	9260.69	5.64E-08	70.84	B		2	1.42	2.35
154	926	A	JA97	24	26	208.24	232.30	3.76	9267.25	9252.5	9263.25	5.41E-08	70.04	B	1		1.32	2.02
154	926	A	JA98	28	30	208.28	232.34	3.80	9269.81	9255.125	9265.81	5.64E-08	68.87	B		2	1.38	2.20
154	926	A	JA99	32	34	208.32	232.38	3.84	9272.38	9257.75	9268.38	5.59E-08	70.55	B	3		1.48	2.10
154	926	A	JA100	36	38	208.36	232.42	3.88	9274.94	9260.375	9270.94	6.06E-08	67.61	B	1		1.48	2.40
154	926	A	JA101	40	42	208.40	232.46	3.92	9277.50	9263	9273.50	6.29E-08	66.37	B		2	1.15	2.28
154	926	A	JA102	44	46	208.44	232.50	3.96	9280.06	9265.625	9276.06	6.49E-08	65.23	B		1	1.32	2.54
154	926	A	JA103	48	50	208.48	232.54	4.00	9282.63	9268.25	9278.63	6.58E-08	66.01	B		2	1.20	2.44
154	926	A	JA104	52	54	208.52	232.58	4.04	9285.19	9270.875	9281.19	6.31E-08	67.05	B	1		1.54	2.28
154	926	A	JA105	56	58	208.56	232.62	4.08	9287.75	9273.5	9283.75	6.50E-08	65.09	B	1		1.35	2.41

154	926	A	JA106	60	62	208.60	232.66	4.12	9290.31	9276.125	9286.31	6.69E-08	65.86					
154	926	A	JA107	64	66	208.64	232.70	4.16	9292.88	9278.75	9288.88	7.53E-08	64.56	A	1		1.27	2.62
154	926	A	JA108	68	70	208.68	232.74	4.20	9295.44	9281.375	9291.44	7.75E-08	63.35	A	1		1.07	2.55
154	926	A	JA109	72	74	208.72	232.78	4.24	9298.00	9284	9294.00	8.69E-08	62.48	B	3		1.34	2.31
154	926	A	JA110	76	78	208.76	232.82	4.28	9300.47	9286.4	9296.53	7.22E-08	64.39	B	1		1.36	2.33
154	926	A	JA111	80	82	208.80	232.86	4.32	9302.93	9288.8	9299.07	6.00E-08	67.61	B	1		1.36	2.39
154	926	A	JA112	84	86	208.84	232.90	4.36	9305.40	9291.2	9301.60	5.37E-08	69.53	B	1	1	1.38	2.52
154	926	A	JA113	88	90	208.88	232.94	4.40	9307.87	9293.6	9304.13	5.11E-08	72.15	B		1	1.36	2.43
154	926	A	JA114	92	94	208.92	232.98	4.44	9310.33	9296	9306.67	4.43E-08	71.81	B	1	1	1.18	2.53
154	926	A	JA115	96	98	208.96	233.02	4.48	9312.80	9298.4	9309.20	5.02E-08	70.27	B		1	1.29	2.37
154	926	A	JA116	100	102	209.00	233.06	4.52	9315.27	9300.8	9311.73	5.12E-08	70.34	B		1	0.93	2.20
154	926	A	JA117	104	106	209.04	233.10	4.56	9317.73	9303.2	9314.27	5.29E-08	68.39	B	1	1	1.27	2.42
154	926	A	JA118	108	110	209.08	233.14	4.60	9320.20	9305.6	9316.80	5.91E-08	66.46	B	1	1	1.28	2.57
154	926	A	JA119	112	114	209.12	233.18	4.64	9322.67	9308	9319.33	6.50E-08	66.11	B		1	0.88	2.67
154	926	A	JA120	116	118	209.16	233.22	4.68	9325.13	9310.4	9321.87	6.21E-08	65.50	B		2	1.13	2.46
154	926	A	JA121	120	122	209.20	233.26	4.72	9327.60	9312.8	9324.40	7.44E-08	62.74					
154	926	A	JA122	124	126	209.24	233.30	4.76	9330.07	9315.2	9326.93	6.20E-08	67.41	B		1	1.25	2.42
154	926	A	JA123	128	130	209.28	233.34	4.80	9332.53	9317.6	9329.47	6.94E-08	65.04	B		1	1.14	2.22
154	926	A	JA124	132	134	209.32	233.38	4.84	9335.00	9320	9332.00	7.43E-08	63.49	B		2	1.22	2.54
154	926	A	JA125	136	138	209.36	233.42	4.88	9337.31	9322.154	9334.26	7.05E-08	66.08	B		2	1.26	2.54
154	926	A	JA126	140	142	209.40	233.46	4.92	9339.62	9324.308	9336.51	6.31E-08	67.82	B		1	0.85	2.57
154	926	A	JA127	144	146	209.44	233.50	4.96	9341.92	9326.462	9338.77	5.56E-08	68.87	B		2	1.29	2.48
154	926	A	JA128	148	150	209.48	233.54	5.00	9344.23	9328.615	9341.03	5.14E-08	73.34	B		2	1.42	2.21
154	926	A	JA129	0	2	209.50	233.56	5.02	9345.38	9329.692	9342.15	4.87E-08	74.02	B		1	1.09	2.17
154	926	A	JA130	4	6	209.54	233.60	5.06	9347.69	9331.846	9344.41	4.40E-08	72.95	B		1		
154	926	A	JA131	8	10	209.58	233.64	5.10	9350.00	9334	9346.67	5.81E-08	66.81	B		2	1.39	2.29
154	926	A	JA132	12	14	209.62	233.68	5.14	9352.31	9336.154	9348.92	5.50E-08	70.07	B		1	1.04	2.24
154	926	A	JA133	16	18	209.66	233.72	5.18	9354.62	9338.308	9351.18	5.66E-08	68.85	B		1	1.44	2.40
154	926	A	JA134	20	22	209.70	233.76	5.22	9356.92	9340.462	9353.44	6.15E-08	68.27	B		3	1.31	2.40
154	926	A	JA135	24	26	209.74	233.80	5.26	9359.23	9342.615	9355.69	6.41E-08	66.07	B		3	1.20	2.37
154	926	A	JA136	28	30	209.78	233.84	5.30	9361.54	9344.769	9357.95	5.75E-08	68.05	B		1	1.25	2.42
154	926	A	JA137	32	34	209.82	233.88	5.34	9363.85	9346.923	9360.21	6.04E-08	65.85	B		1	0.86	2.32
154	926	A	JA138	36	38	209.86	233.92	5.38	9366.15	9349.077	9362.46	5.40E-08	67.22	B		1	1.35	2.34
154	926	A	JA139	40	42	209.90	233.96	5.42	9368.46	9351.231	9364.72	5.61E-08	66.43	B		1	1.08	2.64
154	926	A	JA140	44	46	209.94	234.00	5.46	9370.77	9353.385	9366.97	6.10E-08	68.01					
154	926	A	JA141	48	50	209.98	234.04	5.50	9373.08	9355.538	9369.23	6.79E-08	65.36	B		1	0.98	2.74
154	926	A	JA142	52	54	210.02	234.08	5.54	9375.38	9357.692	9371.49	7.79E-08	59.95	B		2	1.12	2.57
154	926	A	JA143	56	58	210.06	234.12	5.58	9377.69	9359.846	9373.74	7.76E-08	60.31	A	1		1.47	2.35
154	926	A	JA144	60	62	210.10	234.16	5.62	9380.00	9362	9376.00	8.37E-08	62.40					
154	926	A	JA145	64	66	210.14	234.20	5.66	9382.78	9365.444	9379.00	7.44E-08	61.91	B		1	1.42	2.32
154	926	A	JA146	68	70	210.18	234.24	5.70	9385.56	9368.889	9382.00	7.02E-08	64.36	B	1	1	1.27	2.38
154	926	A	JA147	72	74	210.22	234.28	5.74	9388.33	9372.333	9385.00	6.45E-08	65.22	B	1	1	1.09	2.60
154	926	A	JA148	76	78	210.26	234.32	5.78	9391.11	9375.778	9388.00	5.64E-08	69.67	B		1		
154	926	A	JA149	80	82	210.30	234.36	5.82	9393.89	9379.222	9391.00	5.65E-08	69.55				1.00	2.29
154	926	A	JA150	84	86	210.34	234.40	5.86	9396.67	9382.667	9394.00	5.98E-08	68.52	B		1	1.37	2.16
154	926	A	JA151	88	90	210.38	234.44	5.90	9399.44	9386.111	9397.00	6.28E-08	68.42	B		1	1.14	1.97
154	926	A	JA152	92	94	210.42	234.48	5.94	9402.22	9389.556	9400.00	6.30E-08	68.18	B		2	1.36	2.21
154	926	A	JA153	96	98	210.46	234.52	5.98	9405.00	9393	9403.00	6.15E-08	67.77	B		3	1.01	2.30
154	926	A	JA154	100	102	210.50	234.56	6.02	9407.00	9394.9	9404.90	6.45E-08	67.86	B	2		1.22	2.39
154	926	A	JA155	104	106	210.54	234.60	6.06	9409.00	9396.8	9406.80	6.34E-08	68.13	A	1		1.08	2.47
154	926	A	JA156	108	110	210.58	234.64	6.10	9411.00	9398.7	9408.70	5.86E-08	68.92	B		3	1.23	2.31
154	926	A	JA157	112	114	210.62	234.68	6.14	9413.00	9400.6	9410.60	5.20E-08	71.20	B		1	0.94	2.26
154	926	A	JA158	116	118	210.66	234.72	6.18	9415.00	9402.5	9412.50	4.97E-08	70.62	B		1	1.06	2.51
154	926	A	JA159	120	122	210.70	234.76	6.22	9417.00	9404.4	9414.40	4.73E-08	71.84	B		1	0.88	2.49
154	926	A	JA160	124	126	210.74	234.80	6.26	9419.00	9406.3	9416.30	5.02E-08	71.05					

154	926	A	JA161	128	130	210.78	234.84	6.30	9421.00	9408.2	9418.20	5.60E-08	69.55	B		2	1.22	2.39
154	926	A	JA162	132	134	210.82	234.88	6.34	9423.00	9410.1	9420.10	5.66E-08	67.37	B	1		1.19	2.36
154	926	A	JA163	136	138	210.86	234.92	6.38	9425.00	9412	9422.00	7.24E-08	63.62	B	1		1.06	2.25
154	926	A	JA164	140	142	210.90	234.96	6.42	9427.38	9414.19	9424.38	5.77E-08	68.70	B		1	1.04	2.53
154	926	A	JA165	144	146	210.94	235.00	6.46	9429.76	9416.381	9426.76	5.36E-08	69.45					
154	926	A	JA166	148	150	210.98	235.04	6.50	9432.14	9418.571	9429.14	4.60E-08	74.07	B	1		1.29	2.12
154	926	A	JA167	0	2	211.00	235.06	6.52	9433.33	9419.667	9430.33	5.10E-08	70.79	B	1		1.25	2.49
154	926	A	JA168	4	6	211.04	235.10	6.56	9435.71	9421.857	9432.71	5.72E-08	71.42	B		1	0.94	2.01
154	926	A	JA169	8	10	211.08	235.14	6.60	9438.10	9424.048	9435.10	5.99E-08	69.53	B		1	1.08	2.06
154	926	A	JA170	12	14	211.12	235.18	6.64	9440.48	9426.238	9437.48	6.32E-08	67.66	A	1		1.10	2.38
154	926	A	JA171	16	18	211.16	235.22	6.68	9442.86	9428.429	9439.86	6.95E-08	65.50	B		2	1.07	2.34
154	926	A	JA172	20	22	211.20	235.26	6.72	9445.24	9430.619	9442.24	6.50E-08	64.00	B		1	1.40	2.25
154	926	A	JA173	24	26	211.24	235.30	6.76	9447.62	9432.81	9444.62	7.47E-08	63.88	B		1	0.90	2.41
154	926	A	JA174	28	30	211.28	235.34	6.80	9450.00	9435	9447.00	8.03E-08	59.65	B	1	1	1.15	2.51
154	926	A	JA175	32	34	211.32	235.38	6.84	9453.29	9438.429	9449.86	6.85E-08	65.17	B		2	1.34	2.50
154	926	A	JA176	36	38	211.36	235.42	6.88	9456.57	9441.857	9452.71	6.23E-08	66.49	B		1	1.02	2.39
154	926	A	JA177	40	42	211.40	235.46	6.92	9459.86	9445.286	9455.57	6.47E-08	66.04	B		2	1.10	2.52
154	926	A	JA178	44	46	211.44	235.50	6.96	9463.14	9448.714	9458.43	5.95E-08	69.10	A	1		1.19	2.40
154	926	A	JA179	48	50	211.48	235.54	7.00	9466.43	9452.143	9461.29	6.59E-08	66.79	B		2	1.13	2.15
154	926	A	JA180	52	54	211.52	235.58	7.04	9469.71	9455.571	9464.14	8.20E-08	60.93	B		2	1.00	2.25
154	926	A	JA181	56	58	211.56	235.62	7.08	9473.00	9459	9467.00	8.02E-08	61.76	B	1		1.21	2.25
154	926	A	JA182	60	62	211.60	235.66	7.12	9475.56	9461.444	9469.89	8.51E-08	60.99	B	1	1	1.23	2.38
154	926	A	JA183	64	66	211.64	235.70	7.16	9478.11	9463.889	9472.78	6.64E-08	64.29	B		1	1.11	2.36
154	926	A	JA184	68	70	211.68	235.74	7.20	9480.67	9466.333	9475.67	6.28E-08	67.14	B	1	2	1.18	2.38
154	926	A	JA185	72	74	211.72	235.78	7.24	9483.22	9468.778	9478.56	6.48E-08	66.46	B	1	2	1.20	2.21
154	926	A	JA186	76	78	211.76	235.82	7.28	9485.78	9471.222	9481.44	6.24E-08	68.67	B	1		1.16	2.18
154	926	A	JA187	80	82	211.80	235.86	7.32	9488.33	9473.667	9484.33	6.72E-08	68.07	B		3	1.12	2.34
154	926	A	JA188	84	86	211.84	235.90	7.36	9490.89	9476.111	9487.22	7.00E-08	65.73	B	1	2		
154	926	A	JA189	88	90	211.88	235.94	7.40	9493.44	9478.556	9490.11	8.40E-08	64.45				1.16	2.36
154	926	A	JA190	92	94	211.92	235.98	7.44	9496.00	9481	9493.00	8.70E-08	57.70	B		1	0.99	2.45
154	926	A	JA191	96	98	211.96	236.02	7.48	9499.00	9484.571	9496.14	1.06E-07	58.02	B	1	1	0.84	2.48
154	926	B	JB1	14	16.5	211.14	235.71	7.42	9494.56	9479.625	9491.38	9.65E-08	64.44	B		3	0.92	2.54
154	926	B	JB2	20	22	211.20	235.77	7.48	9499.00	9484.571	9496.14	1.03E-07	56.49	B	1	1	1.21	2.20
154	926	B	JB3	24	26	211.24	235.81	7.52	9502.00	9488.143	9499.29	7.95E-08	61.05	B	1	2	1.09	2.35
154	926	B	JB4	28	29.5	211.28	235.85	7.56	9505.00	9491.714	9502.43	6.52E-08	68.23	B	1	2	1.28	2.15
154	926	B	JB5	32	34	211.32	235.89	7.60	9508.00	9495.286	9505.57	7.14E-08	67.46	B		1	0.83	2.24
154	926	B	JB6	36	38	211.36	235.93	7.64	9511.00	9498.857	9508.71	7.02E-08	65.65	A		2	1.16	2.24
154	926	B	JB7	40	42	211.40	235.97	7.68	9514.00	9502.429	9511.86	6.98E-08	68.46	B		1	0.94	2.27
154	926	B	JB8	44	46	211.44	236.01	7.72	9517.00	9506	9515.00	7.38E-08	66.71	B		5	0.95	2.40
154	926	B	JB9	48	50	211.48	236.05	7.76	9519.88	9506	9517.63	6.97E-08	64.89	B		6	1.01	2.41
154	926	B	JB10	52.5	54.5	211.53	236.10	7.81	9523.11	9506	9520.58	7.28E-08	62.33	B		3	0.87	2.45
154	926	B	JB11	56.5	58.5	211.57	236.14	7.85	9525.98	9506	9523.20	6.91E-08	63.12	B		7	0.59	2.56
154	926	B	JB12	60.5	62.2	211.61	236.18	7.89	9528.86	9506	9525.83	6.16E-08	65.43	B		5	0.61	2.47
154	926	B	JB13	64	66	211.64	236.21	7.92	9531.38	9506	9528.13	7.49E-08	61.55	C		2	0.45	2.27
154	926	B	JB14	68	70	211.68	236.25	7.96	9534.25	9506.001	9530.75	7.55E-08	63.24	B		1	0.91	2.44
154	926	B	JB15	72	74	211.72	236.29	8.00	9537.13	9506.001	9533.38	8.81E-08	58.49	B		2	1.19	2.42
154	926	B	JB16	76	78	211.76	236.33	8.04	9540.00	9506.001	9536.00	1.06E-07	57.49	B	1		1.26	2.22
154	926	B	JB17	81.5	83.5	211.82	236.39	8.10	9543.76	9506.001	9539.91	7.85E-08	63.15	B		3	0.94	2.51
154	926	B	JB18	85.5	87.5	211.86	236.43	8.14	9546.50	9506.001	9542.75	4.91E-08	69.41	B	1	1	1.12	2.30
154	926	B	JB19	91.5	93.5	211.92	236.49	8.20	9550.61	9506.001	9547.01	5.31E-08	70.62	B	3		1.22	2.22
154	926	B	JB20	95.5	97.5	211.96	236.53	8.24	9553.34	9506.001	9549.86	5.11E-08	70.44					
154	926	B	JB21	99.5	101.3	212.00	236.57	8.28	9556.08	9506.001	9552.70	5.05E-08	68.68	C		2	0.76	2.44
154	926	B	JB22	103	105	212.03	236.60	8.31	9558.47	9506.001	9555.18	5.76E-08	68.42					
154	926	B	JB23	107	109	212.07	236.64	8.35	9561.21	9506.001	9558.03	6.60E-08	66.22	B		3	0.61	2.59
154	926	B	JB24	111	112	212.11	236.68	8.39	9563.95	9506.001	9560.87	8.35E-08	59.97	A	1		1.11	2.38

154	926	B	JB25	114	116	212.14	236.71	8.42	9566.00	9506.001	9563.00	8.54E-08	63.33	B	3		1.01	2.46
154	926	B	JB26	118	120	212.18	236.75	8.46	9568.58	9506.002	9565.58	8.30E-08	61.65	A	4		1.00	2.55
154	926	B	JB27	122	124	212.22	236.79	8.50	9571.16	9506.002	9568.16	4.72E-08	66.96	B	3		1.10	2.45
154	926	B	JB28	126	127.3	212.26	236.83	8.54	9573.74	9506.002	9570.74	6.47E-08	63.97	B		1	0.87	2.41
154	926	B	JB29	129.5	131.5	212.30	236.87	8.58	9576.00	9506.002	9573.00	7.08E-08	64.67	B	1	3	0.98	2.40
154	926	B	JB30	133.5	135.5	212.34	236.91	8.62	9578.58	9506.002	9575.58	7.50E-08	63.69	B		5	0.97	2.53
154	926	B	JB31	137.5	139.5	212.38	236.95	8.66	9581.16	9506.002	9578.16	6.77E-08	64.60	B	2	1	0.63	2.59
154	926	B	JB32	141.5	143.5	212.42	236.99	8.70	9583.74	9506.002	9580.74	7.44E-08	63.49	B		2	1.09	2.28
154	926	B	JB33	145.5	147.5	212.46	237.03	8.74	9586.28	9506.002	9583.27	8.00E-08	62.43	B	1		1.18	2.43
154	926	B	JB34	5.5	8.6	212.56	237.13	8.84	9591.79	9506.002	9588.57	5.00E-08	67.67	B	2		1.20	2.22
154	926	B	JB35	10.5	12.5	212.61	237.18	8.89	9594.54	9506.002	9591.22	4.35E-08	72.43	B	1	3	1.14	2.18
154	926	B	JB36	14	16.3	212.64	237.21	8.92	9596.47	9506.003	9593.08	2.44E-08	74.82					
154	926	B	JB37	18	20	212.68	237.25	8.96	9598.67	9506.003	9595.20	4.57E-08	72.31	B		3	0.70	2.21
154	926	B	JB38	22	24	212.72	237.29	9.00	9600.88	9506.003	9597.33	5.13E-08	70.33	B		3	1.06	2.08
154	926	B	JB39	26	28	212.76	237.33	9.04	9603.08	9506.003	9599.45	5.34E-08	68.89	B	1	3	1.06	2.10
154	926	B	JB40	31	33	212.81	237.38	9.09	9605.84	9506.003	9602.10	5.23E-08	69.50	B	1	2	0.89	2.27
154	926	B	JB41	35	37	212.85	237.42	9.13	9608.04	9506.003	9604.22	5.26E-08	70.76	B		4	1.01	2.27
154	926	B	JB42	39	41	212.89	237.46	9.17	9610.24	9506.003	9606.35	8.35E-08	60.37	C		2	0.69	2.21
154	926	B	JB43	43	45	212.93	237.50	9.21	9612.45	9506.003	9608.47	9.75E-08	57.53	B		2	1.03	2.27
154	926	B	JB44	47	49	212.97	237.54	9.25	9613.98	9506.003	9611.42	9.17E-08	56.71	B	4		1.03	2.33
154	926	B	JB45	51	53	213.01	237.58	9.29	9615.29	9506.003	9614.65	5.77E-08	65.85	B		5	0.77	2.53
154	926	B	JB46	55	57	213.05	237.62	9.33	9616.60	9506.003	9617.88	6.30E-08	68.32	B		4	1.02	2.34
154	926	B	JB47	60.5	62.5	213.11	237.68	9.39	9618.39	9506.003	9622.33	5.91E-08	67.25	B		6	0.61	2.39
154	926	B	JB48	64.5	66.5	213.15	237.72	9.43	9619.70	9506.004	9625.56	5.95E-08	68.05	B		4	0.62	2.38
154	926	B	JB49	68.5	70.5	213.19	237.76	9.47	9621.01	9506.004	9628.79	6.30E-08	68.02	B		5	1.14	2.24
154	926	B	JB50	72.5	74.5	213.23	237.80	9.51	9622.32	9506.004	9632.02	5.73E-08	68.64	B		5	1.12	2.14
154	926	B	JB51	78.5	80.5	213.29	237.86	9.57	9624.28	9506.004	9636.87	6.45E-08	62.47	B		5	0.95	2.12
154	926	B	JB52	82.5	84.5	213.33	237.90	9.61	9625.59	9506.004	9640.10	6.47E-08	61.45	B		7	0.97	2.32
154	926	B	JB53	86.5	88.5	213.37	237.94	9.65	9626.89	9506.004	9643.33	6.49E-08	64.51	B	5		0.86	2.17
154	926	B	JB54	93	95	213.43	238.00	9.71	9629.02	9506.004	9648.58	6.40E-08	63.00	B		4	0.71	2.53
154	926	B	JB55	97	99	213.47	238.04	9.75	9630.78	9506.004	9651.60	6.87E-08	61.88	B	2	2	1.04	2.34
154	926	B	JB56	101	103	213.51	238.08	9.79	9633.89	9506.004	9654.00	6.43E-08	63.27	B	2		0.87	2.48
154	926	B	JB57	105	107	213.55	238.12	9.83	9637.01	9506.004	9656.40	7.47E-08	64.24	B	3		1.05	2.44
154	926	B	JB58	109	111	213.59	238.16	9.87	9640.12	9506.005	9658.80	7.55E-08	57.82	B	2		0.92	3.07
154	926	B	JB59	113	115	213.63	238.20	9.91	9643.24	9506.005	9661.20	6.56E-08	64.85	B	3		1.10	2.32
154	926	B	JB60	117	119	213.67	238.24	9.95	9646.35	9506.005	9663.60	5.61E-08	67.86	B	6		1.12	2.26
154	926	B	JB61	121	123	213.71	238.28	9.99	9649.46	9506.005	9666.00	4.83E-08	71.34	B	1	2	0.12	2.59
154	926	B	JB62	125	126.3	213.75	238.32	10.03	9652.58	9506.005	9668.40	4.71E-08	72.12	B	3		1.15	2.22
154	926	B	JB63	128	130	213.78	238.35	10.06	9654.91	9506.005	9670.20	4.74E-08	71.51	B	1	2	1.14	2.20
154	926	B	JB64	132	134	213.82	238.39	10.10	9658.03	9506.005	9672.60	4.74E-08	72.11	BA	2		1.23	2.34
154	926	B	JB65	136	138	213.86	238.43	10.14	9661.14	9506.005	9675.00	4.80E-08	71.04	B	1	2	1.20	2.07
154	926	B	JB66	140	142	213.90	238.47	10.18	9664.26	9506.005	9677.40	4.81E-08	71.68	B		2	1.24	2.11
154	926	B	JB67	146	148	213.96	238.53	10.24	9668.93	9506.005	9681.00	5.02E-08	71.84	B		4	1.21	2.22
154	926	B	JB68	0	2	214.00	238.57	10.28	9672.04	9506.005	9683.40	5.04E-08	68.22	B	1	1	0.57	2.42
154	926	B	JB69	4	6	214.04	238.61	10.32	9675.16	9506.005	9685.80	4.89E-08	71.85	B	2	1	0.95	2.03
154	926	B	JB70	8	10	214.08	238.65	10.36	9678.27	9506.006	9688.20	5.05E-08	70.59	B	1		1.16	1.93
154	926	B	JB71	12	14	214.12	238.69	10.40	9681.39	9506.006	9690.60	4.83E-08	69.44	B	1	2	1.14	2.17
154	926	B	JB72	16	17	214.16	238.73	10.44	9684.50	9506.006	9693.00	4.58E-08	71.96	B	1	1	1.00	2.20
154	926	B	JB73	20	22	214.20	238.77	10.48	9687.61	9506.006	9695.40	5.86E-08	68.73	B		2	1.08	2.32
154	926	B	JB74	24	26	214.24	238.81	10.52	9690.73	9506.006	9697.80	6.05E-08	68.58	A	3		1.25	2.34
154	926	B	JB75	28	29.7	214.28	238.85	10.56	9693.84	9506.006	9700.20	6.04E-08	67.24	A	4		1.20	2.25
154	926	B	JB76	31.8	34	214.32	238.89	10.60	9696.80	9506.006	9702.48	5.51E-08	68.87	B	1		1.13	2.08
154	926	B	JB77	36	38	214.36	238.93	10.64	9700.07	9506.006	9705.00	5.84E-08	69.69	B	2	1	1.26	2.19
154	926	B	JB78	40	42	214.40	238.97	10.68	9703.19	9506.006	9707.40	6.43E-08	66.24	A	1	1	0.82	2.14
154	926	B	JB79	44	46	214.44	239.01	10.72	9706.30	9506.006	9709.80	6.48E-08	68.18	B	1		1.27	2.15

154	926	B	JB80	49	51	214.49	239.06	10.77	9710.19	9506.006	9712.80	5.82E-08	69.51	B	1	1	0.97	2.27
154	926	B	JB81	53	55	214.53	239.10	10.81	9713.31	9506.006	9715.20	5.30E-08	71.99	B		5	1.17	2.10
154	926	B	JB82	57	59	214.57	239.14	10.85	9716.42	9506.007	9717.60	5.39E-08	71.73	B	1	1	1.35	2.03
154	926	B	JB83	61	63	214.61	239.18	10.89	9719.54	9506.007	9720.00	5.66E-08	68.36	B	3		1.27	2.01
154	926	B	JB84	65	66.6	214.65	239.22	10.93	9722.65	9506.007	9722.40	6.27E-08	65.53	B	3		1.24	2.22
154	926	B	JB85	68.5	70.5	214.69	239.26	10.97	9725.38	9506.007	9724.50	6.72E-08	64.89	B	3		1.18	2.29
154	926	B	JB86	72.5	74.5	214.73	239.30	11.01	9728.49	9506.007	9726.90	6.58E-08	67.31	B	1		0.88	2.32
154	926	B	JB87	76.5	78.5	214.77	239.34	11.05	9731.60	9506.007	9729.30	6.93E-08	67.22	B	3		1.07	2.34
154	926	B	JB88	80	82	214.80	239.37	11.08	9734.33	9506.007	9731.40	7.77E-08	61.87	B	1	1	1.08	2.36
154	926	B	JB89	84	86	214.84	239.41	11.12	9737.44	9506.007	9733.80	9.25E-08	62.00	B		1	0.91	2.32
154	926	B	JB90	88	90	214.88	239.45	11.16	9740.14	9506.007	9736.26	9.10E-08	60.35	B	1	1	1.21	2.31
154	926	B	JB91	92	94	214.92	239.49	11.20	9742.43	9506.007	9738.77	6.04E-08	66.72	B	1		1.23	2.26
154	926	C	JC1	24	26	220.74	239.65	11.15	9739.57	9506.007	9735.63	7.23E-08	62.87	B	3		1.21	2.33
154	926	C	JC2	28	30	220.78	239.69	11.19	9741.86	9506.007	9738.14	5.99E-08	68.46	B		2	1.30	2.19
154	926	C	JC3	32	34	220.82	239.73	11.23	9744.14	9506.007	9740.66	5.32E-08	71.25	B	1	2	1.11	2.25
154	926	C	JC4	36	38	220.86	239.77	11.27	9746.43	9506.007	9743.17	4.85E-08	69.59	B		2	1.25	2.17
154	926	C	JC5	40	42	220.90	239.81	11.31	9748.71	9506.008	9745.69	4.54E-08	73.54	B	2		1.31	2.01
154	926	C	JC6	44	46	220.94	239.85	11.35	9751.00	9506.008	9748.20	4.78E-08	70.13	B	1	2	1.25	2.14
154	926	C	JC7	48	50	220.98	239.89	11.39	9753.29	9506.008	9750.71	4.91E-08	73.40	B		1	0.79	2.09
154	926	C	JC8	52	54	221.02	239.93	11.43	9755.57	9506.008	9753.23	5.78E-08	69.28	B	1	2	1.09	2.15
154	926	C	JC9	56	58	221.06	239.97	11.47	9757.86	9506.008	9755.74	6.16E-08	68.10	B	4		1.31	2.13
154	926	C	JC10	60	62	221.10	240.01	11.51	9760.10	9506.008	9758.05	5.80E-08	69.25	B	3		1.23	2.15
154	926	C	JC11	64	66	221.14	240.05	11.55	9762.30	9506.008	9760.15	5.74E-08	67.99	B	3		1.08	2.10
154	926	C	JC12	68	70	221.18	240.09	11.59	9764.50	9506.008	9762.25	5.60E-08	68.65	B	4		1.24	2.07
154	926	C	JC13	72	74	221.22	240.13	11.63	9766.70	9506.008	9764.35	5.58E-08	67.73	B	2		1.15	2.07
154	926	C	JC14	76	78	221.26	240.17	11.67	9768.90	9506.008	9766.45	5.07E-08	68.84	B	4		1.06	2.13
154	926	C	JC15	80	82	221.30	240.21	11.71	9771.10	9506.008	9768.55	5.40E-08	69.67	B	2		0.95	2.05
154	926	C	JC16	84	86	221.34	240.25	11.75	9773.30	9506.008	9770.65	6.05E-08	68.67	B	2		1.07	2.36
154	926	C	JC17	88	90	221.38	240.29	11.79	9775.50	9506.009	9772.75	7.00E-08	63.73	B	2		1.08	2.12
154	926	C	JC18	92	94	221.42	240.33	11.83	9777.70	9506.009	9774.85	6.96E-08	61.46	B	1	1	0.98	2.23
154	926	C	JC19	96	98	221.46	240.37	11.87	9779.90	9506.009	9776.95	8.88E-08	61.73	B	3		0.90	2.30
154	926	C	JC20	100	102	221.50	240.41	11.91	9782.11	9506.009	9779.16	8.31E-08	61.39	B	2		1.13	2.22
154	926	C	JC21	104	106	221.54	240.45	11.95	9784.32	9506.009	9781.47	8.03E-08	64.30	B	2		1.23	2.08
154	926	C	JC22	108	110	221.58	240.49	11.99	9786.53	9506.009	9783.79	5.85E-08	69.86	B	3		1.04	2.35
154	926	C	JC23	112	114	221.62	240.53	12.03	9788.74	9506.009	9786.11	5.78E-08	69.49	B	1		1.20	2.17
154	926	C	JC24	116	118	221.66	240.57	12.07	9790.95	9506.009	9788.42	5.88E-08	70.31	B	1		0.63	1.80
154	926	C	JC25	120	122	221.70	240.61	12.11	9793.16	9506.009	9790.74	6.50E-08	67.69	B	2		1.33	1.92
154	926	C	JC26	124	126	221.74	240.65	12.15	9795.37	9506.009	9793.05	6.93E-08	64.94	B	3		1.34	1.95
154	926	C	JC27	128	130	221.78	240.69	12.19	9797.58	9506.009	9795.37	7.36E-08	65.67	B	2		1.29	2.07
154	926	C	JC28	132	134	221.82	240.73	12.23	9799.79	9506.009	9797.68	7.93E-08	63.17	B	2		1.21	2.12
154	926	C	JC29	136	138	221.86	240.77	12.27	9802.00	9506.01	9800.00	8.27E-08	63.53	B	2		1.20	2.11
154	926	C	JC30	140	142	221.90	240.81	12.31	9804.49	9506.01	9802.27	7.80E-08	63.81	B			1.22	2.15
154	926	C	JC31	144	146	221.94	240.85	12.35	9806.97	9506.01	9804.54	6.93E-08	64.86	B	2		1.08	2.04
154	926	C	JC32	148	150	221.98	240.89	12.39	9809.46	9506.01	9806.81	5.89E-08	66.87	B	3		1.24	2.21
154	926	C	JC33	0	2	222.00	240.91	12.41	9810.70	9506.01	9807.95	6.45E-08	64.10	B	1		1.01	2.07
154	926	C	JC34	4	6	222.04	240.95	12.45	9813.19	9506.01	9810.22	6.39E-08	63.97	B	2		1.19	2.21
154	926	C	JC35	8	10	222.08	240.99	12.49	9815.68	9506.01	9812.49	7.40E-08	62.71	B		1	0.73	2.28
154	926	C	JC36	12	14	222.12	241.03	12.53	9818.16	9506.01	9814.76	8.30E-08	61.74	B	1		1.28	2.07
154	926	C	JC37	16	18	222.16	241.07	12.57	9820.65	9506.01	9817.03	8.40E-08	60.02	B	1		1.09	2.38
154	926	C	JC38	20	22	222.20	241.11	12.61	9823.14	9506.01	9819.30	9.78E-08	59.35	B	1		1.17	2.44
154	926	C	JC39	24	26	222.24	241.15	12.65	9825.53	9506.01	9821.53	9.56E-08	58.12	B	2		1.14	2.21
154	926	C	JC40	28	30	222.28	241.19	12.69	9827.64	9506.01	9823.64	9.03E-08	59.61	A	1		1.12	2.28
154	926	C	JC41	32	34	222.32	241.23	12.73	9829.75	9506.011	9825.75	7.13E-08	63.62	B	5		1.17	2.12
154	926	C	JC42	36	38	222.36	241.27	12.77	9831.87	9506.011	9827.87	5.47E-08	67.91	B	3		1.18	2.22
154	926	C	JC43	40	42	222.40	241.31	12.81	9833.98	9506.011	9829.98	4.87E-08	72.38	B	4		1.24	2.09

154	926	C	JC44	44	46	222.44	241.35	12.85	9836.09	9506.011	9832.09	4.67E-08	72.29	B	2		1.26	2.01
154	926	C	JC46	48	50	222.48	241.39	12.89	9838.21	9506.011	9834.21	6.00E-08	67.31	B	2		1.18	2.02
154	926	C	JC45	52	54	222.52	241.43	12.93	9840.32	9506.011	9836.32	4.94E-08	69.69	B	3		1.16	1.94
154	926	C	JC47	56	58	222.56	241.47	12.97	9842.43	9506.011	9838.43	5.93E-08	67.15	B	1		0.93	2.05
154	926	C	JC48	60	62	222.60	241.51	13.01	9844.55	9506.011	9840.55	6.75E-08	62.97	B		2	0.97	2.29
154	926	C	JC49	64	66	222.64	241.55	13.05	9846.66	9506.011	9842.66	6.77E-08	65.25	B	1	1	0.77	2.16
154	926	C	JC50	68	70	222.68	241.59	13.09	9848.77	9506.011	9844.77	9.93E-08	57.38	B	1		0.95	2.41
154	926	C	JC51	72	74	222.72	241.63	13.13	9850.89	9506.011	9846.89	8.89E-08	58.45	B	2		1.06	2.35
154	926	C	JC52	76	78	222.76	241.67	13.17	9853.00	9506.011	9849.00	1.14E-07	55.74	B	2		1.06	2.38
154	926	C	JC53	80	82	222.80	241.71	13.21	9857.71	9506.012	9853.94	9.84E-08	59.79	B		3	1.11	2.25
154	926	C	JC54	84	86	222.84	241.75	13.25	9862.41	9506.012	9858.88	6.50E-08	64.33	B		6	1.05	2.28
154	926	C	JC55	88	90	222.88	241.79	13.29	9867.12	9506.012	9863.82	8.23E-08	63.77	B		2	1.09	2.32
154	926	C	JC56	92	94	222.92	241.83	13.33	9871.82	9506.012	9868.76	8.42E-08	62.70	B	6		1.22	1.99
154	926	C	JC57	96	98	222.96	241.87	13.37	9874.60	9506.012	9871.60	8.48E-08	61.22	B	2		1.20	1.85
154	926	C	JC58	100	102	223.00	241.91	13.41	9876.74	9506.012	9873.74	8.53E-08	61.97	B	2		1.19	1.96
154	926	C	JC59	104	106	223.04	241.95	13.45	9878.88	9506.012	9875.88	7.28E-08	63.01	B		3	1.11	2.15
154	926	C	JC60	108	110	223.08	241.99	13.49	9881.02	9506.012	9878.02	5.86E-08	68.12	B	4		1.10	2.02
154	926	C	JC61	112	114	223.12	242.03	13.53	9883.16	9506.012	9880.16	6.11E-08	66.78	B	3		0.83	1.84
154	926	C	JC62	116	118	223.16	242.07	13.57	9885.30	9506.012	9882.30	6.56E-08	66.17	B	2		0.96	1.97
154	926	C	JC63	120	122	223.20	242.11	13.61	9887.44	9506.012	9884.44	7.47E-08	61.52	B	2		0.64	1.95
154	926	C	JC64	124	126	223.24	242.15	13.65	9889.58	9506.012	9886.58	9.23E-08	58.36	B	1		0.98	1.95
154	926	C	JC65	128	130	223.28	242.19	13.69	9891.72	9506.013	9888.72	1.07E-07	51.79	B	1		1.01	2.39
154	926	C	JC66	132	134	223.32	242.23	13.73	9893.86	9506.013	9890.86	1.25E-07	48.11	B		2	0.85	2.21
154	926	C	JC67	136	138	223.36	242.27	13.77	9896.00	9506.013	9893.00	1.43E-07	47.81	B		1	0.60	2.43
154	926	C	JC68	140	142	223.40	242.31	13.81	9899.08	9506.013	9896.08	1.12E-07	53.83	B	3		1.06	2.29
154	926	C	JC69	144	146	223.44	242.35	13.85	9902.15	9506.013	9899.15	6.86E-08	67.54	B	2		1.21	2.10
154	926	C	JC70	148	150	223.48	242.39	13.89	9905.23	9506.013	9902.23	6.31E-08	69.68	B		1	1.04	2.11
154	926	C	JC71	0	2	223.50	242.41	13.91	9906.77	9506.013	9903.77	6.73E-08	66.15	B	3		1.07	1.99
154	926	C	JC72	4	6	223.54	242.45	13.95	9909.85	9506.013	9906.85	8.01E-08	63.72	B	3		1.21	2.10
154	926	C	JC73	8	10	223.58	242.49	13.99	9912.92	9506.013	9909.92	9.01E-08	60.09	B	2		1.19	2.08
154	926	C	JC74	12	14	223.62	242.53	14.03	9916.00	9506.013	9913.00	1.00E-07	60.14	B	2		1.32	1.99
154	926	C	JC75	16	18	223.66	242.57	14.07	9919.71	9506.013	9916.57	7.09E-08	66.08	B		2	1.24	2.21
154	926	C	JC76	20	22	223.70	242.61	14.11	9923.43	9506.013	9920.14	5.71E-08	68.54	B	2		1.35	2.01
154	926	C	JC77	24	26	223.74	242.65	14.15	9927.14	9506.014	9923.71	5.41E-08	69.98	B	3		1.04	2.13
154	926	C	JC78	28	30	223.78	242.69	14.19	9930.86	9506.014	9927.29	5.67E-08	67.29	B		1	0.84	2.41
154	926	C	JC79	32	34	223.82	242.73	14.23	9934.57	9506.014	9930.86	7.13E-08	61.54	B	2		1.14	2.07
154	926	C	JC80	36	38	223.86	242.77	14.27	9938.29	9506.014	9934.43	1.14E-07	53.81	B		2	0.94	2.37
154	926	C	JC81	40	42	223.90	242.81	14.31	9942.00	9506.014	9938.00	1.51E-07	50.41	B		1	0.95	2.48
154	926	C	JC82	44	46	223.94	242.85	14.35	9945.33	9506.014	9941.47	1.27E-07	53.43	B	1		1.09	2.36
154	926	C	JC83	48	50	223.98	242.89	14.39	9948.67	9506.014	9944.93	8.91E-08	57.88	B	2		1.23	2.06
154	926	C	JC84	52	54	224.02	242.93	14.43	9952.00	9506.014	9948.40	6.23E-08	68.77	B		1	1.16	2.14
154	926	C	JC85	56	58	224.06	242.97	14.47	9955.33	9506.014	9951.87	6.44E-08	70.42	B	1		0.87	2.07
154	926	C	JC86	60	62	224.10	243.01	14.51	9958.67	9506.014	9955.33	7.62E-08	66.21	B	3		1.19	2.01
154	926	C	JC87	64	66	224.14	243.05	14.55	9962.00	9506.014	9958.80	6.83E-08	67.73	B	3		1.16	2.09
154	926	C	JC88	68	70	224.18	243.09	14.59	9965.33	9506.014	9962.27	1.13E-07	56.09	B	3		1.17	1.99
154	926	C	JC89	72	74	224.22	243.13	14.63	9968.62	9506.015	9965.62	1.13E-07	56.22	B		1	0.85	2.19
154	926	C	JC90	76	78	224.26	243.17	14.67	9971.85	9506.015	9968.85	9.68E-08	59.07	B	1		1.09	2.21
154	926	C	JC91	80	82	224.30	243.21	14.71	9975.08	9506.015	9972.08	7.59E-08	61.08	B	1		1.15	2.30
154	926	C	JC92	84	86	224.34	243.25	14.75	9978.31	9506.015	9975.31	5.36E-08	70.52	B		2	0.92	2.20
154	926	C	JC93	88	90	224.38	243.29	14.79	9981.54	9506.015	9978.54	5.95E-08	67.64	B	1		1.06	2.03
154	926	C	JC94	92	94	224.42	243.33	14.83	9984.77	9506.015	9981.77	8.33E-08	65.20	B	1		1.08	2.13
154	926	C	JC95	96	98	224.46	243.37	14.87	9988.00	9506.015	9985.00	1.01E-07	57.87	B	1		1.04	2.07
154	926	C	JC96	100	102	224.50	243.41	14.91	9991.14	9506.015	9988.14	4.33E-08	71.70	B		2	1.02	2.13
154	926	C	JC97	104	106	224.54	243.45	14.95	9994.29	9506.015	9991.29	4.33E-08	73.47	B		2	0.82	2.02
154	926	C	JC98	108	110	224.58	243.49	14.99	9997.43	9506.015	9994.43	4.67E-08	72.52	B	3		1.07	1.92

154	926	C	JC99	112	114	224.62	243.53	15.03	10000.57	9506.015	9997.57	5.18E-08	70.18	B	1		0.49	1.71
154	926	C	JC100	116	118	224.66	243.57	15.07	10003.71	9506.015	10000.71	6.20E-08	67.58	B		3	0.94	2.09
154	926	C	JC101	120	122	224.70	243.61	15.11	10006.86	9506.016	10003.86	8.99E-08	60.98	B		1	0.84	2.37
154	926	C	JC102	124	126	224.74	243.65	15.15	10010.00	9506.016	10007.00	1.05E-07	56.86	B		1	0.76	2.45
* A=>355mu, B=250-355mu, C=150-250mu, D=63-150mu																		
** If >1 forams are crushed before measuring																		

Appendix 2. All data